Journal of Geodynamics 158 (2023) 102005

Contents lists available at ScienceDirect

Journal of Geodynamics

journal homepage: www.elsevier.com/locate/jog

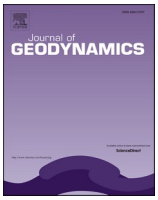

Revisiting the geodynamics of the Middle East region from an integrated geophysical perspective

Chiara Civiero [a,b,*], Nicolas L. Celli [c], Magdala Tesauro [a,d]

[a] Dipartimento di Matematica e Geoscienze, Università di Trieste, Trieste, Italy
[b] Institut de Ciències del Mar, ICM-CSIC, Barcelona, Spain
[c] Dublin Institute for Advanced Studies (DIAS), Dublin D02 Y006, Ireland
[d] University of Utrecht, Department of Geosciences, Netherlands

ARTICLE INFO

Keywords:
Mantle flow
Azimuthal anisotropy
Seismic Tomography
Lithospheric thickness
Mantle plumes
Upwelling-induced traction

ABSTRACT

A long-standing question in geodynamics is whether mantle flow is driven by the plate motion alone, or mantle upwelling makes a significant contribution to it. Subducting slabs and lateral variations of the continental lithosphere can further influence the asthenospheric flow and control its direction. The Middle East region (MER) is a complex continental setting where different processes such as rifting, break-up, plate collision, and tectonic escape kinematically interact with each other. In this context, the role that lithospheric structure, mantle flow, and active upwellings may play is debated. Tomographic images provide a snapshot of the current thermal conditions of a region and seismic anisotropy can also help resolve mantle convection. Here, we synthesize shear-wave splitting observations together with up-to-date tomography models of the mantle structure beneath the MER and other geophysical data. Low-velocity anomalies are seen at asthenospheric depths beneath W Arabia, NW Iran, and Anatolia, suggesting a spreading zone of warm mantle. Two deep low-velocity bodies in Afar and Levant –interpreted as hot mantle plumes– are the sources of this shallower mantle flow. Where low velocities are imaged, we observe predominantly NE–SW oriented anisotropy, anomalously high topography, and abundant basaltic volcanism. The integrated analysis suggests that a horizontal component associated with active upwelling is present in the upper-mantle flow field. The large-scale circulation flow fed by the Afar and Levant Plumes, aided by the subduction-induced forces, facilitates the lateral motion of the Anatolian microplate and affects the dynamic evolution of the Zagros orogen. The proposed scenario demonstrates that the interplay between plate-tectonic events and mantle dynamics controls the kinematics of the region and can explain the general patterns of deformation observed at the surface.

1. Introduction

The relationship between continental tectonics and mantle convection is an outstanding problem in geodynamics that has been extensively studied in the past (e.g., Bercovici et al., 2000; Forte et al., 2010; Liu et al., 2004; Ricard and Vigny, 1989; Turcotte and Oxburgh, 1972; Zhong and Gurnis, 1995). Continental lithosphere has a longer deformation history and a more complex upper-mantle viscosity structure than its oceanic counterpart. While the oceanic lithosphere has a relatively uniform thickness (for age older than 80 Ma), the continental lithosphere features significant spatial variations in thickness, which translate into large lateral changes in viscosity affecting the mantle flow field beneath it (Artemieva and Mooney, 2002; Conrad et al., 2007; Fouch et al., 2000; Fouch and Rondenay, 2006). Where the lithosphere is thin and weak, the pattern of the underlying mantle convection can influence the surface topography and volcanism emplacement (Turcotte and Schubert, 2002). Asthenospheric flow can be exerted by convective structures such as mantle plumes, which manifest a horizontal flow component when they reach the bottom of the lithosphere (e.g., Behn et al., 2004; Sleep, 1997). If the overlying lithosphere is sufficiently thin, such mantle plumes can also join to each other by hot sheets creating a continuous radial flow, which can deform the surface broadly and generate large-scale gravity anomalies (Lees et al., 2020; McKenzie, 2020; White, 1988).

The Middle East region (MER) offers an excellent place to study the pattern of the horizontal mantle flow associated with active upwelling,

* Corresponding author at: Dipartimento di Matematica e Geoscienze, Università di Trieste, Trieste, Italy.
E-mail address: chiara.civiero@units.it (C. Civiero).

https://doi.org/10.1016/j.jog.2023.102005
Received 1 September 2023; Received in revised form 28 October 2023; Accepted 21 November 2023
Available online 24 November 2023

due to the presence of prominent asthenospheric low seismic velocities, and a variable lithospheric structure and topography (Chorowicz, 2005; Hansen et al., 2012; Stern and Johnson, 2010). The MER is divided into a series of continental plates (i.e., Arabian, Anatolian, Iranian, and African plates) that are in relative motion with respect to each other and show different patterns of lithospheric deformation. The extent to which these tectonic plates are coupled to mantle flow has been investigated by using a range of different approaches (e.g., Faccenna et al., 2013; Faccenna and Becker, 2010; Komut, 2015; Mousavi et al., 2023; Şengül Uluocak et al., 2021; Wei et al., 2019). However, a great deal of work remains in understanding the underlying mantle convection dynamics and its impact on the lithosphere, as well as plate motion, surface topography, and volcanism.

Constraints on the upper-mantle structure below different domains of the MER have been provided by seismic tomographic imaging studies using both body waves (e.g., Amini et al., 2012; Koulakov et al., 2016; Kounoudis et al., 2020; Park et al., 2008, 2007; Portner et al., 2018; Shomali et al., 2011; Tang et al., 2019, 2016; Wei et al., 2019) and surface waves (e.g., Kaviani et al., 2020; Salaün et al., 2012; Tang et al., 2018, 2016). The resulting tomographic models resolve the main heterogeneities of the 3D velocity structure and, in some cases, have been used to interpret the mantle dynamic impact in relation to the variable lithospheric architecture and surface tectonics, as measured in terms of dynamic topography and mantle flow (e.g., Behn et al., 2004; Faccenna et al., 2013). However, although such tomography models can provide a snapshot of the present-day thermal state of the mantle, they alone do not yield any information on the pattern of sub-continental mantle flow at a large scale and its connection with the deeper mantle.

Inferences on the character of the mantle flow field can be derived from seismic anisotropy measurements, where the orientation of observed anisotropy is taken as a direct indicator of the flow direction (Becker et al., 2008; Fouch and Rondenay, 2006; Holtzman et al., 2003; Ribe, 1989; Wang and Becker, 2019). Previous shear-wave splitting analyses on the MER revealed that seismic anisotropy occurs in the lithosphere or asthenosphere (e.g., Biryol et al., 2010; Gao et al., 2022; Hansen et al., 2006; Kaviani et al., 2021, 2009; Paul et al., 2014; Qaysi et al., 2018; Sadeghi-Bagherabadi et al., 2018; Salah, 2013; Sandvol et al., 2003; Wolfe et al., 1999). The main challenge in the interpretation of any anisotropy results is the relatively poor depth constraint on the source of the undergoing anisotropy (Long and Silver, 2009). Anisotropy can originate in the asthenosphere when the relative motion between the plates and underlying mantle is accommodated, while mantle lithosphere is not actively deforming because of its strength. In contrast, plate deformation may induce lithospheric anisotropy in areas of active rifting or orogeny (e.g., Park and Levin, 2002). Consequently, different (and often mutually exclusive) geodynamic models have been proposed to explain the mantle deformation patterns of the MER (Balázs et al., 2021; Confal et al., 2018; Faccenna et al., 2013; Le Pichon and Kreemer, 2010; Sadeghi-Bagherabadi et al., 2018; Zhu et al., 2022). Comparison of seismic anisotropy with tomography images of the upper mantle together with other multi-disciplinary data is a helpful approach to address this ambiguity and make the anisotropy observations and their relationship with the mantle flow field more meaningful (Becker et al., 2012).

In this study, we utilize images from a recent regional waveform tomography model along with observables from seismic anisotropy and other geophysical information to give new insights into the dynamic processes of the mantle beneath the Middle East system. By taking advantage of the increasing number of studies published over the last decades, we first present an overview of the geophysical data available for the entire region, showing additional results from new residual topography and velocity-temperature calculations. We then interpret them and outline specific points of discussion such as the origin of mantle flow and coupling between the moving lithospheric plates and the underlying mantle. By reviewing this large amount of observations, we will give an updated perspective on the pattern of mantle convection below the region and understand how active upwelling flow interacts with the forces driving continental plate motions.

2. Tectonic background

The kinematics of the MER is influenced by the northward movement of Arabia with respect to Eurasia (McKenzie, 1970) (Fig. 1). The Zagros Mountains and Iranian Plateau were formed as a result of the continental collision of the Arabian Plate with Eurasia that started ~16–23 Ma and was preceded by long-lasting oceanic subduction of the Neotethys Ocean (Hatzfeld and Molnar, 2010; Robertson, 2000; Sengör and Kidd, 1979). The NW–SE trending Zagros fold-and-thrust belt (ZFTB), which extends over about 2000 km from Turkey through SW Iran, marks the deformational front on the passive margin of the Arabian Plate (Berberian, 1995; Mouthereau, 2011). To the east, the Iranian Plateau is made up of microblocks derived from northern Gondwana (McQuarrie and Van Hinsbergen, 2013) and the strike-slip movement between them accommodates part of the convergence (Vernant et al., 2004). The paucity of seismicity recorded in the area (Fig. 2A) implies a lack of deformation, i.e., a quasi-rigid behaviour of these aseismic blocks relative to the intensely active seismic belts that surround them (Jackson and McKenzie, 1988). This plateau is located between the Alborz Orogen in the north and the Makran Subduction Zone in the south. The active Alborz mountain belt stretches over 900 km along the southern margin of the South Caspian Basin and can be divided into eastern, central, and western parts (Zanchi et al., 2009). The Makran Subduction Zone extends from SE Iran to southern Pakistan and includes an accretionary wedge, where the Tethys oceanic lithosphere on the Arabian Plate is subducting beneath the Eurasian Plate (Byrne et al., 1992).

Moving to the west, the Anatolian Plateau is the result of the amalgamation of major lithospheric blocks during the Cretaceous Tethyan subduction (Şengör and Yilmaz, 1981; Van Hinsbergen et al., 2016). Currently, it comprises three main neotectonic domains, namely the East Anatolian Plateau, Central Anatolian Plateau, and Western Anatolian Province (Fig. 1). South of the East Anatolian Plateau, the Bitlis Suture represents the terminal boundary between the Eurasian and Arabian plates formed during the closure of the Neotethys Ocean (Agard et al., 2005). The Bitlis Suture connects to the Main Zagros Thrust, which separates the seismic ZFTB from the almost aseismic Central Iran (Talebian and Jackson, 2002).

Within the Mediterranean domain, subduction of the African lithosphere beneath the Western Anatolian Province and Central Anatolian Plateau contribute to the western escape of the Anatolian block via strike-slip conjugate motions along the Northern Anatolian fault and Eastern Anatolian fault zones (Şengör et al., 2005). In the Late Eocene, the Arabian plate started to split from the African plate along the Red Sea and the Gulf of Aqaba regions (Hempton, 1987). This divergence has been affected by the Afar hotspot located at the triple junction between the Red Sea rift, Gulf of Aden, and Main Ethiopian rift in NE Africa (Mohr, 1970). Arabia's continued northward motion and further separation from the African plate along the left-lateral strike-slip Dead Sea Fault (Smit et al., 2010) in the Miocene-Pliocene resulted in a faster movement of Arabia compared to Africa (Fig. 1).

The GPS coverage of the MER has significantly improved over the past two decades and we now have more detailed information about present-day kinematics. Our updated GPS compilation of velocity data (Khorrami et al., 2019; Serpelloni et al., 2022; Tunini et al., 2017) provides a complete overview of the first-order regional kinematics of the plate interactions and its relation with the mantle dynamic forces (Fig. 2B). The most evident observation is the counterclockwise motion relative to Eurasia, which encompasses Arabia, Anatolia, and Aegean (Şengör et al., 2005). While the Arabia rotation has been going on at a steady rate since ~40 Ma, the Anatolia rotation is younger and initiated less than 12 Ma (Le Pichon et al., 1995).

The overall pattern of deformation is controlled by the motion of the Arabian Plate from the divergence along the Red Sea rift to the

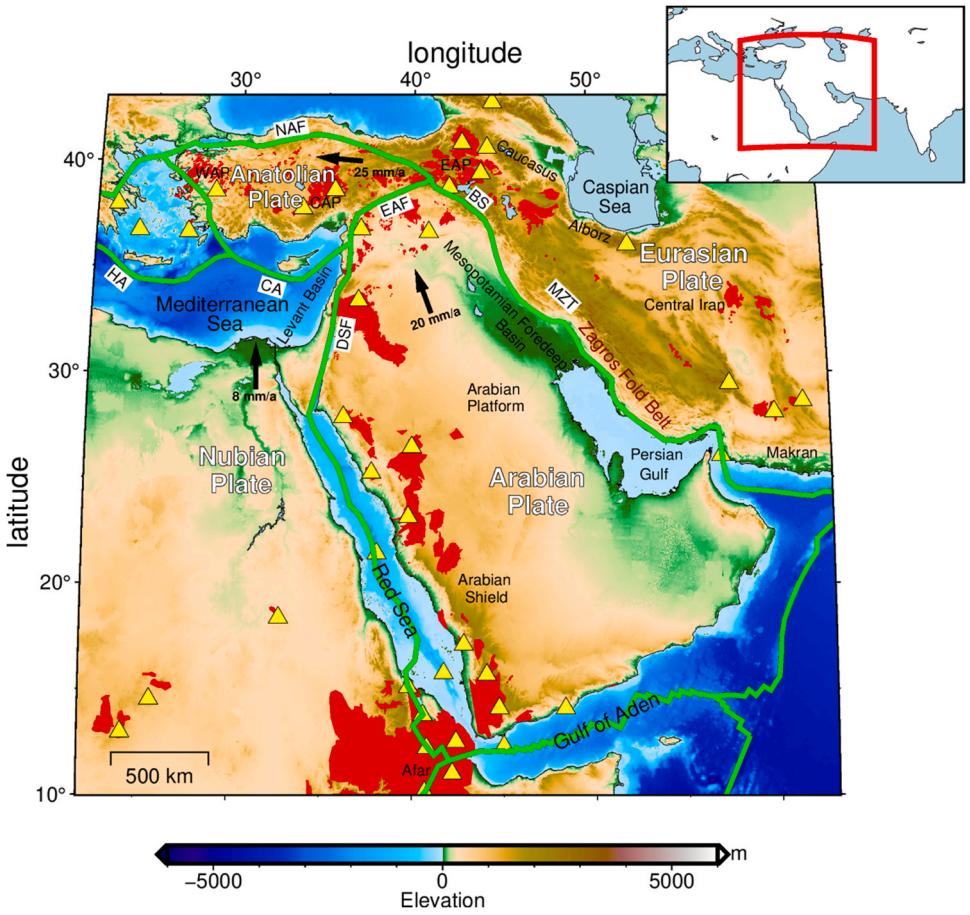

Fig. 1. Simplified tectonic map of the Middle East region. WAP—Western Anatolian province; CAP—Central Anatolian Plateau; EAP—East Anatolian Plateau; BS—Bitlis suture; DSF—Dead Sea fault; NAF—Northern Anatolian fault; EAF—Eastern Anatolian fault; MZT—Main Zagros Thrust; CA—Cyprus Arc; HA—Hellenic Arc. The Cenozoic intraplate basaltic volcanism is displayed in red. Yellow triangles represent Quaternary volcanoes. Plate boundaries are shown as green lines. Inset: Location of the study area limited by a red box.

convergence in the north along the Zagros collision zone. Part of this convergence is, however, deviated toward the Hellenic subduction through the westward extrusion of Anatolia along the Northern Anatolian fault, due to the tendency of the continental lithosphere to move laterally away from zones of compression (Mckenzie, 1972; Reilinger et al., 1997). Although inferences about the forces driving deformation cannot be made based solely on kinematics, the widespread coherency of the young Anatolian circular velocity pattern and the increase in movement rates toward the Hellenic-Cyprus arc suggest a ductile mantle control rather than a simple push by the Arabian Plate (Le Pichon and Kreemer, 2010). These forces could be attributed to the mantle suction exerted by the retreating Hellenic subducting slab or convective processes in the mantle, acting on the base of the plate (i.e., mantle flow or drag).

3. Regional upper-mantle tomography of the Middle East region

Knowledge of the upper-mantle structure beneath the MER comes from numerous tomographic models. Regional travel-time imaging studies of northern East Africa clearly show a strong, vertical low-velocity feature extending through the mantle transition zone (MTZ) beneath Ethiopia (e.g., Bastow et al., 2008; Benoit et al., 2006; Chang and Van der Lee, 2011; Civiero et al., 2019a, 2016; Hammond et al., 2013; Hansen and Nyblade, 2013). According to continental (e.g., Boyce et al., 2021; Hansen et al., 2012) and global tomography images (e.g., Montelli et al., 2004; Ritsema et al., 1999), the anomaly originates from the lower mantle and impinges upon the Afro-Arabian lithosphere in the Afar triple junction zone. This low-velocity feature appears to propagate northward at shallow asthenospheric depths beneath the Red Sea and the Arabian Shield (Al-Lazki et al., 2004; Amini et al., 2012; Civiero et al., 2022; Koulakov et al., 2016; Lim et al., 2020; Park et al., 2008; Tang et al., 2019; Wei et al., 2019; Yao et al., 2017).

Variations in shear-wave velocity in the upper mantle are mainly due to changes in temperature and, to a lesser extent, compositional heterogeneities (as well as by the presence of volatiles and partial melt). The strong low shear-wave velocities imaged below northern East Africa and western Arabia coincide with areas of elevated surface topography and recent basaltic volcanism oriented NNW–SSE (Fig. 1). Given the stronger sensitivity of the seismic velocities to temperature than composition (e.g., Deschamps and Trampert, 2003), the upper mantle in this region is likely above the solidus temperature and has been interpreted as due to hot mantle material, which deflects horizontally from the Afar Plume and flows northward in the asthenosphere through corridors of relatively thin lithosphere, causing continental intraplate volcanism above it (Chang et al., 2011; Civiero et al., 2022; Ebinger and Sleep, 1998).

Sesimic attenuation maps (Gök et al., 2003; Kaviani et al., 2022) as well as P- (Amini et al., 2012; Hearn and Ni, 1994; Kounoudis et al., 2020; Portner et al., 2018) and S-wave models (Kaviani et al., 2020; Maggi and Priestley, 2005; Manaman et al., 2011; Rahimi et al., 2014; Skobeltsyn et al., 2014) reveal that the Anatolian and Iranian Plateaus are also underlain by low-wave velocity anomalies indicating relatively hot and weak upper mantle with a thin lithosphere. In contrast, P- and S-wave high-velocity anomalies commonly imaged beneath the Arabian

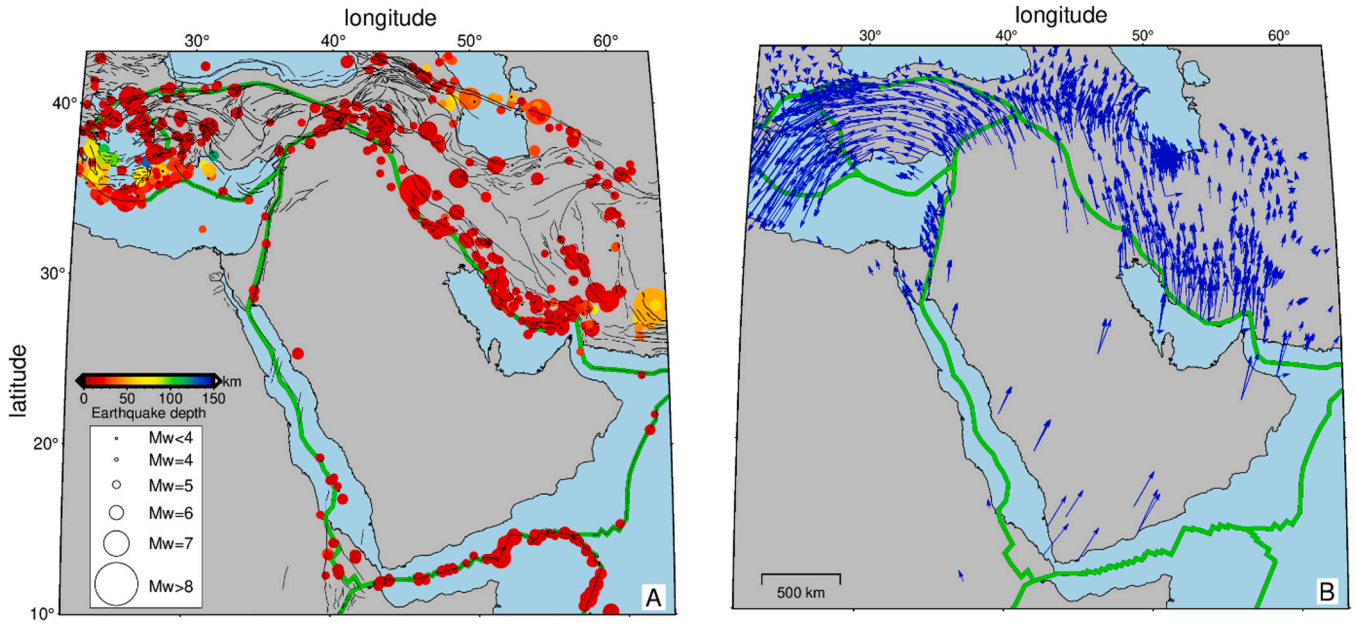

Fig. 2. A. Seismicity and seismogenic faulting of the Middle East region. The earthquakes are taken from the GEM-ISC catalogue (Di Giacomo et al., 2018; Storchak et al., 2015, 2013). The size of the circle determines the magnitude of the event while the color indicates the depth. The crustal faults are downloaded from the GEM Global Active Faults Database (Styron and Pagani, 2020). B. Horizontal GPS velocities, which include the compilations and studies of Khorrami et al. (2019); Serpelloni et al. (2022); and Tunini et al. (2017). Note the spectacular counterclockwise rotation of the Arabian plate, Iran, Turkey, and Aegea relative to Eurasia. Plate boundaries are shown as green lines.

Platform (Kim et al., 2023; Koulakov et al., 2016; Lim et al., 2020; Park et al., 2008; Yao et al., 2017) and Zagros relative to Central Iran (Alinaghi et al., 2007; Al-Lazki et al., 2004; Maggi and Priestley, 2005; Paul et al., 2010; Rahmani et al., 2019; Wei et al., 2019) suggest the presence of a thicker and colder lithosphere. Recently, Mousavi and Fullea (2020) using gravity, topography, and petrological data have modeled a 250-km-thick lithosphere beneath Zagros, thinning up to ~100 km beneath the Iranian Plateau. A slightly lower value of lithospheric thickness (70 km) has been estimated for the Iranian Plateau by Kaviani et al. (2020).

The mantle structure beneath the Levant domain is less investigated by seismic tomography compared to the adjacent regions. High-resolution regional and continental-scale imaging studies of P and S waves show pronounced low-velocity anomalies in the upper mantle but imaged in different locations, below Syria and Jordan and at the border between Iraq and Saudi Arabia (Alinaghi et al., 2007; Boyce et al., 2021; Chang et al., 2010; Chang and Van der Lee, 2011; Civiero et al., 2022; Hansen et al., 2012). A recent stochastic inversion of surface-wave dispersion measurements has associated the low shear-wave velocities found beneath the Levant Basin and eastwards with a thin, ~75 km thick continental lithosphere (El-Sharkawy et al., 2021). Currently, it is still unclear if and how these features relate to the asthenospheric low-velocity corridor in the south.

3.1. *New structural features from the AF2019 waveform model*

In Figs. 3 and 4 we show the most up-to-date shear-wave velocity model of the lithosphere and underlying upper mantle of the entire region of study, called *AF2019*, which has been computed applying waveform inversion to extract structural information from surface and regional S and multiple S waves (Celli et al., 2020). This model has been extended and updated in the recent work of Civiero et al. (2022) to include Anatolia and the Southern Caucasus. In this paper, we use the extended *AF2019* model to focus on several intriguing—and previously undiscussed— structural features, which lead us to make new inferences for the geodynamics of the region, especially in the northern Middle East and Zagros collision system. A series of resolution spike tests, placing input anomalies at different depths and locations, confirms that the model can resolve the upper-mantle structure accurately despite some smearing of the output anomalies, especially within the MTZ (Fig. 5). We also perform an additional structural resolution test where we remove the low-velocity structure beneath northern East Africa, western Arabia, and the Levant region in the input model (Fig. 6). Despite a weak ($dV_S < -1\%$) spurious feature in the Levant, all the recovered images do not show any low-velocity features, as expected. Further and more complex resolution tests are shown in Civiero et al. (2022).

The most striking feature observed in the map views of Fig. 3 is the continuous low-velocity channel from Ethiopia in the African Plate to western Arabia, Syria, and Anatolia at depths < 250 km, previously interpreted as one branch of the broad, star-shaped plume head centered below Afar (Civiero et al., 2022). Looking deeper, the model reveals a strong, roundish low-velocity feature in the MTZ beneath Iraq, surrounded by the N–NW by high-velocity anomalies correlated with thicker lithosphere. The cross-sections AA' and BB' in Fig. 4 show that such a feature extends from the base of the upper mantle beneath Iraq up to Syria at shallower depths and it is in contact with the fast east-Arabia lithosphere. These suggest the presence of another hot mantle upwelling, called the Levant Plume, which impinges onto the thick and cold lithosphere of the Arabian Platform and deflects westward, into the thin-lithosphere channel, feeding most of the Mesopotamian volcanism (Civiero et al., 2022). Interestingly, we observe a high coherence between the negative deep upper-mantle anomaly and the significantly thin MTZ (~230 km) found in the P-wave receiver functions study of Kaviani et al. (2018), pointing out a thermal anomaly (i.e., mantle upwelling) that crosses the 410- and 660-km discontinuities.

In Turkey, a widespread low-velocity anomaly at depths less than 200 km beneath the high elevations of the Central and East Anatolian Plateaus merges with that in the Levant and NW Iran (Fig. 3, cross-sections EE' and FF' in Fig. 4). To the west, the most prominent feature in the uppermost mantle is the high-velocity anomaly coincident with the Hellenic trench domain. At deeper depths (> 300 km), we observe that the high velocities connect with those present around the Zagros and resemble a continuous NNE-dipping subduction slab. However, within the MTZ this high-velocity body breaks up into two pieces,

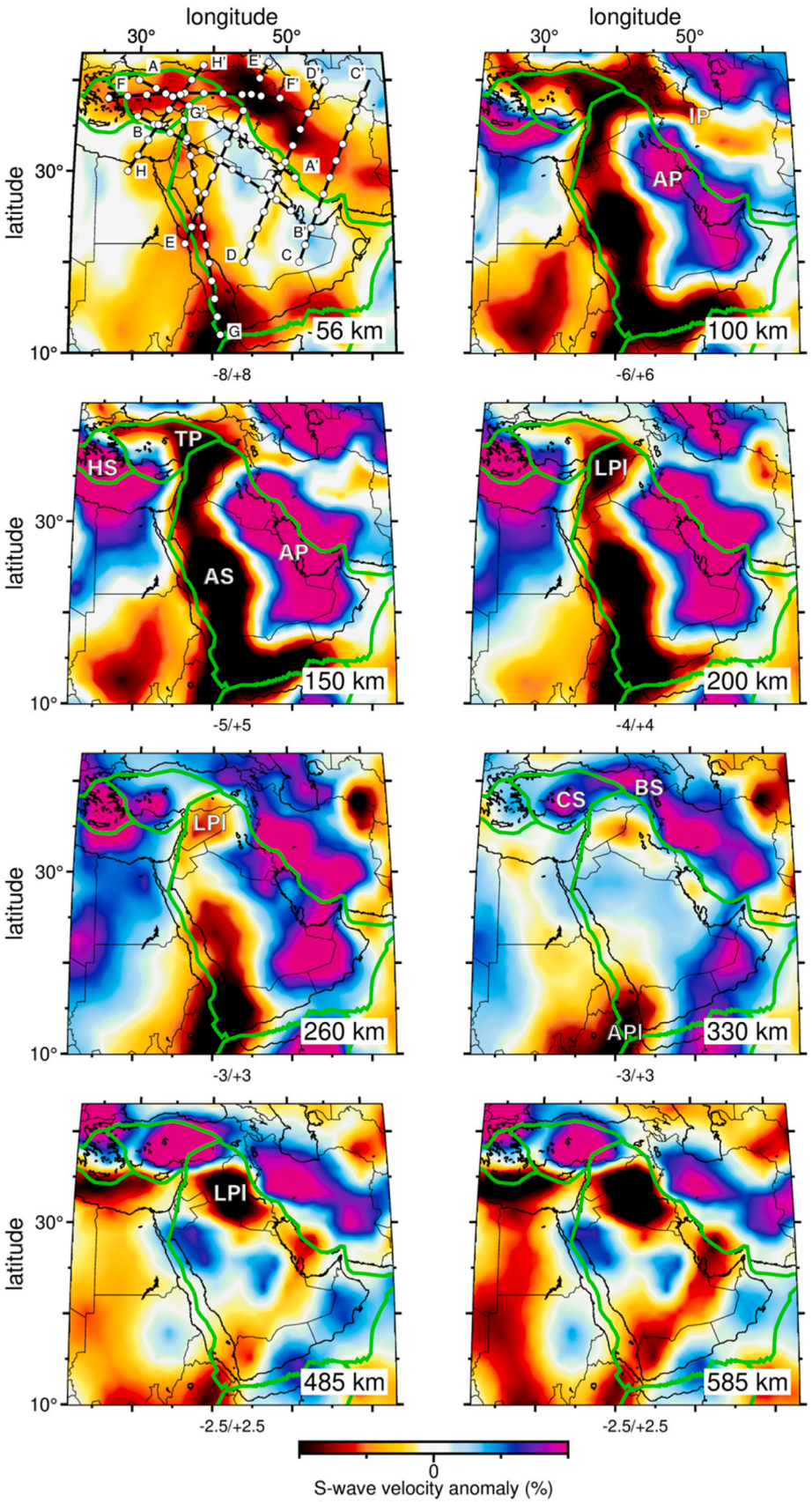

Fig. 3. Map views of the extended *AF2019* model at eight different depths. The velocity anomalies are plotted relative to the reference value at each depth, taken from the reference model of the tomographic inversion. The colour scale limit varies with depth and is given at the bottom of each frame. AP: Arabian Platform; APl: Afar Plume; AS: Arabian Shield; BS. Bitlis subduction; CS: Cyprus subduction; HS: Hellenic subduction; IP: Iranian Plateau; LPl: Levant Plume; TP: Turkish (or Anatolian) Plateau. Plate boundaries are shown as green lines. The locations of the cross-sections in Fig. 4 are displayed as black lines in the 56-km depth map.

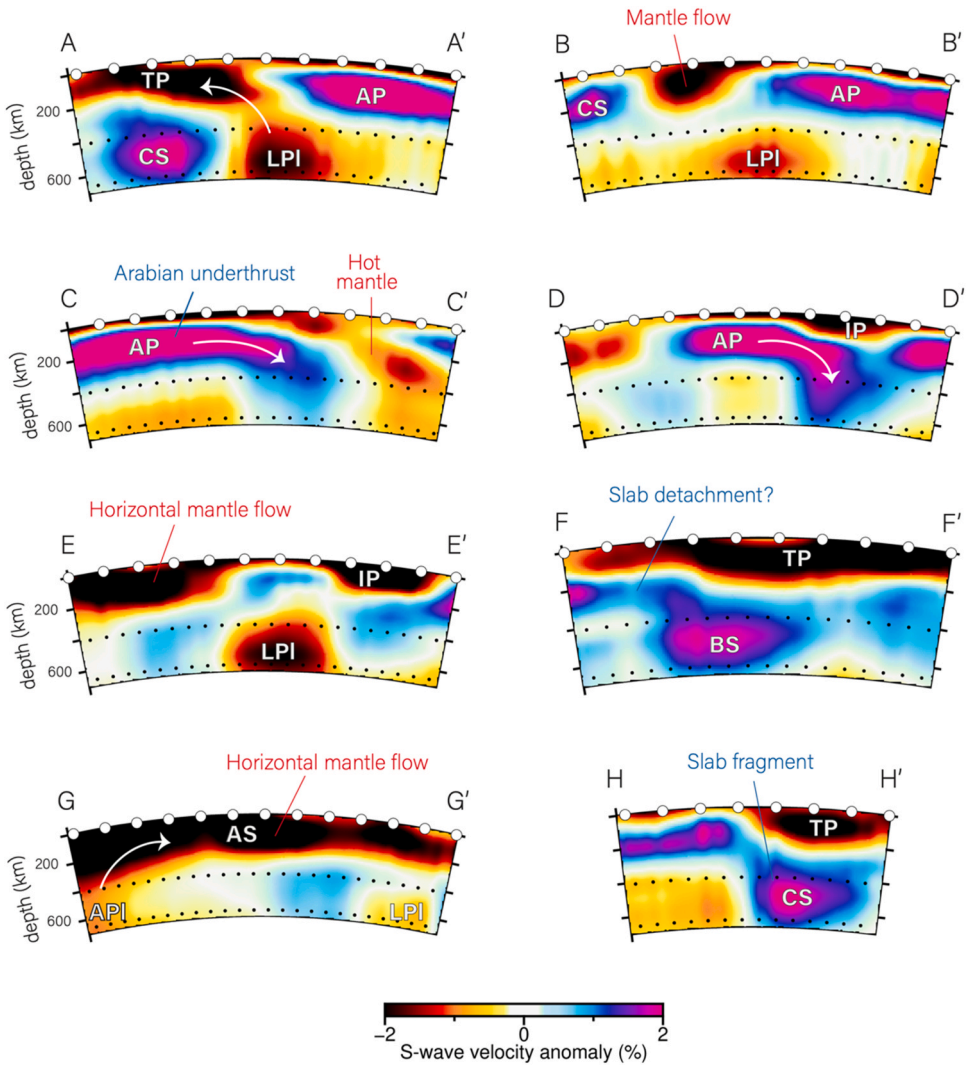

Fig. 4. Eight vertical cross sections through the model. The locations of the cross-sections are displayed as black lines in the 56-km depth map in Fig. 3. White points indicate the distance every 2°. The MTZ discontinuities at 410- and 660-km depth are indicated by black points. Cross-section A-A' cuts through the tilted Levant Plume (LPl). B-B' shows the cold Arabian Platform (AP) and the adjacent asthenospheric mantle flow from Levant Plume (LPl) and Afar Plume (Apl). Sections C-C' and D-D' cross the high-velocity anomaly interpreted as the Arabian margin underthrusting Iran in N and S Zagros, respectively. Section E-E' shows the Levant Plume tail and the hot mantle beneath the Iranian Plateau. Section F-F' provides a view of the low-velocity channel below the Turkish Plateau (TP) and the detached Bitlis subduction (BS). Section G-G' cuts the Afar Plume in East Africa and the low-velocity channel flowing northward beneath the Arabian Shield (AS). Note that the low-velocity channel beneath Anatolia and W Arabia is continuous in the shallowest upper mantle. Section H-H' shows a fragment of the Cyprus slab (CS) lying at the base of the MTZ.

one lying beneath Anatolia (see Fig. 3 and cross-section HH' in Fig. 4) and one in Iran, where the slab appears continuous down to the base of the model (cross-sections CC' and DD', Fig. 4). The weakening of the anomaly starting at ~300 km depth likely indicates a slab detachment. The Bitlis domain is dominated by low-velocity perturbations at depths above ~250 km while an isolated high-velocity body is imaged below (cross-section FF', Fig. 4).

Eastwards, a strong high-velocity anomaly appears beneath the Zagros Mountains, which merges with that imaged beneath the thick Arabian Platform at depths less than 300 km. According to the cross-sections CC' and DD' of Fig. 4, this feature dips NE-ward extending throughout the upper mantle. A similar feature has been imaged in previous P-wave tomography inversions (Rahmani et al., 2019; Shomali et al., 2011; Veisi et al., 2021), but down to shallower depths.

We now convert the seismic velocities dV_S to temperature anomalies following the method described in Civiero et al. (2019b). The velocity anomalies could be the effect of the temperature variations and chemical composition, as well as of partial melt, water, grain size, and seismic anisotropy. However, if we assume that the effect of composition on seismic velocity in the upper mantle is secondary to that of temperature (Cammarano et al., 2003), we can interpret the seismic velocity structure solely in terms of temperature. Here, we use a smooth (isomorphic) dV_S/dT derivative for a pyrolytic composition along a 1300° adiabat (Styles et al., 2011). Errors in the derivative lead to uncertainties in temperature anomalies of a few tens of degrees (Cammarano et al., 2003; Goes et al., 2000). In Fig. 7 we show the temperature anomalies in the uppermost mantle, at 110 and 260 km depth, respectively. As expected, the highest positive thermal contrasts are observed below Africa, western Arabia, and the Levant region with a peak of ~300 °C beneath Afar and the Arabian Shield. These very high temperatures imply that also other effects (e.g., partial melt and volatiles) may have a contribution to explain the low-velocity seismic anomalies. Beneath Syria, where a low-velocity anomaly interpreted as a mantle upwelling is imaged, we also observe a temperature excess of ~100–200 °C.

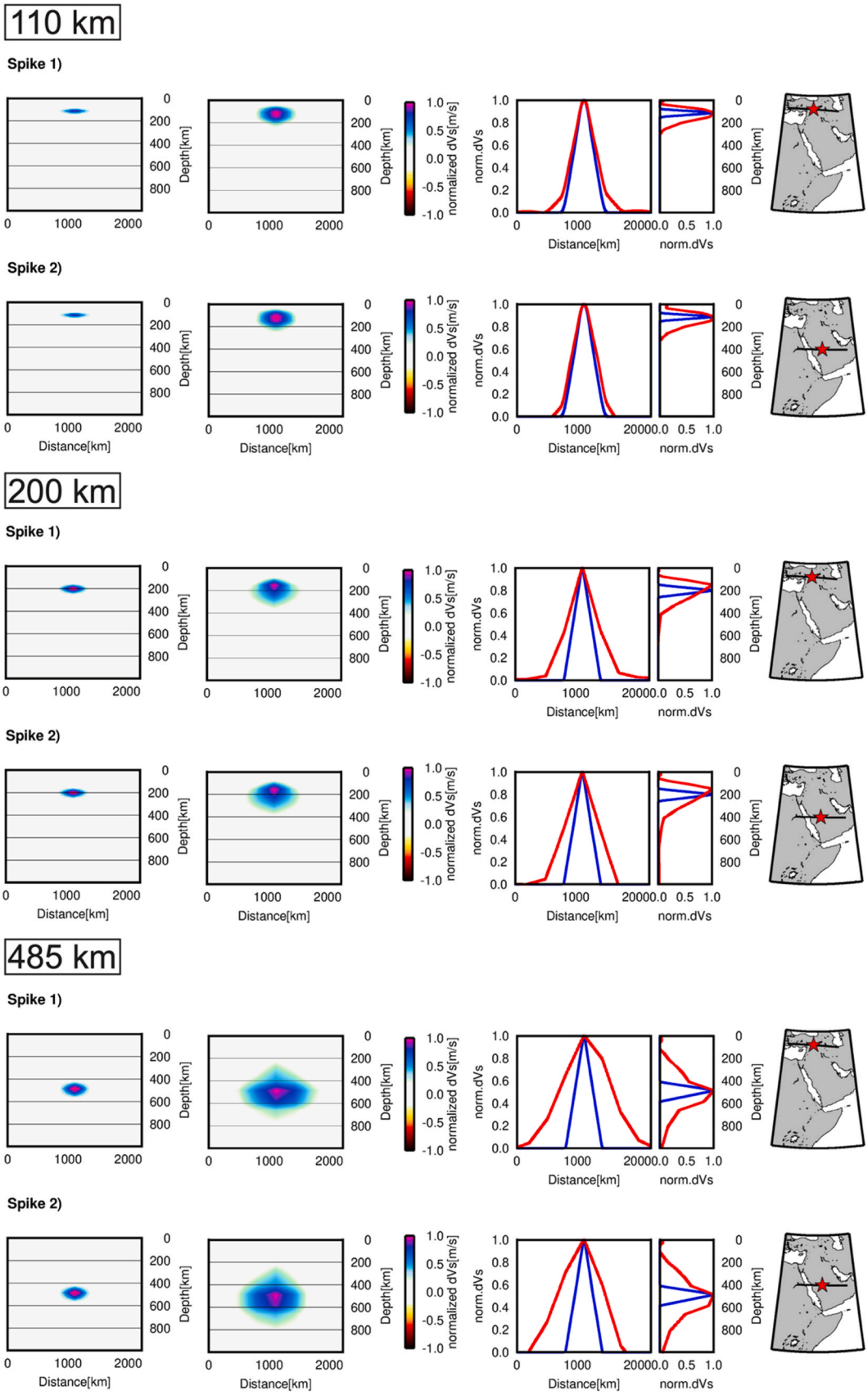

Fig. 5. Spike resolution tests. Spikes' location is shown on the map on the right as red stars. The input spikes are placed at 110, 200 and 485 km depth. For each spike we plot a vertical cross-section through the input (first panel) and output (second panel) models. The orientation of the profile is shown on the map in black. The third and fourth panels indicate horizontal and vertical 1-D S-wave anomaly profiles along the cross-section. Input profiles are shown in blue, and output in red. All S-wave velocity anomalies are normalized to the maximum.

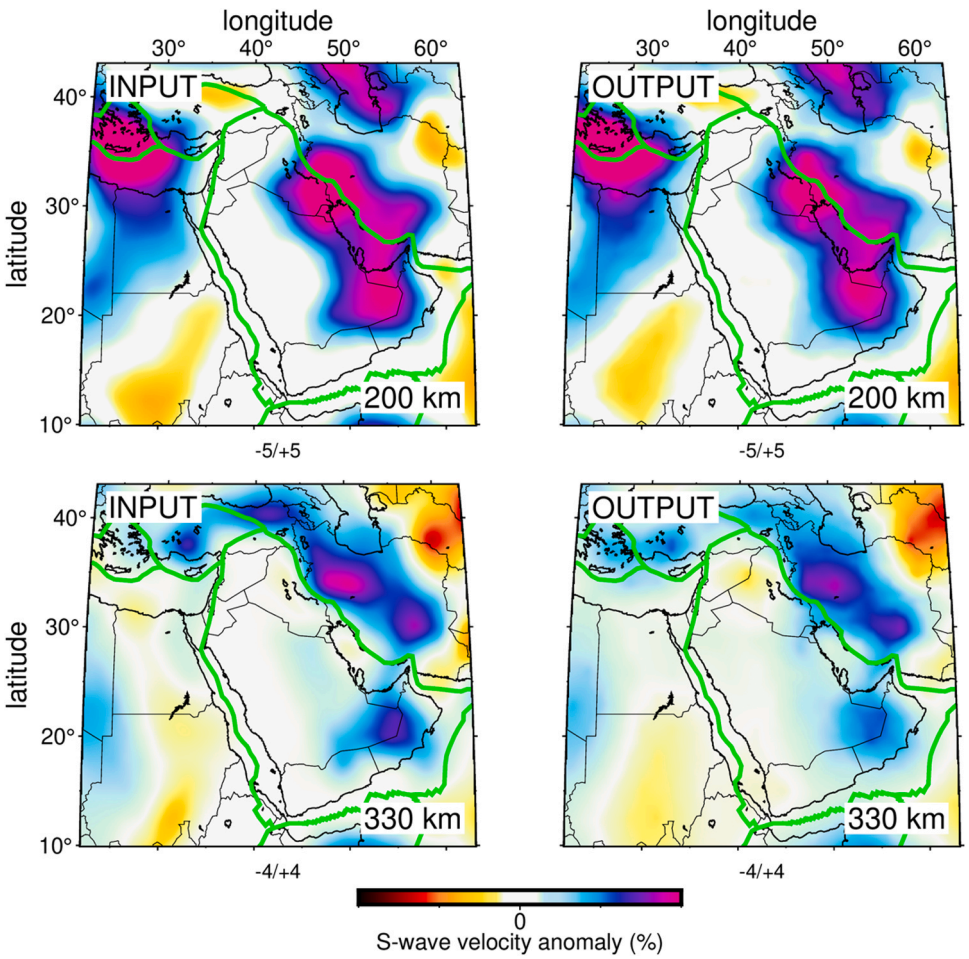

Fig. 6. Structural resolution test where the low-velocity channel beneath the Arabian Shield and Levant region is removed in the input (left panels, top: 200 km depth; bottom: 330 km depth). In the recovered models (right panels) the low velocities are absent and only a weak spurious low-velocity feature (magnitude < –1%) appears beneath Iraq at 330 km depth. Plate boundaries are shown as green lines.

3.2. *Comparison with global tomography models*

As mentioned before, the upper-mantle low-velocity anomaly imaged in the Levant region has been identified previously in a few other regional tomography models (Alinaghi et al., 2007; Chang et al., 2010; Chang and Van der Lee, 2011; Kaviani et al., 2020; Kim et al., 2023; Koulakov et al., 2016) but slightly offset compared to our images. To confirm the occurrence and location of this new key feature in the *AF2019* model, we compare the upper-mantle model with three global whole-mantle P-wave models and three global S-wave models.

The three global teleseismic P-wave models are UU-P07 (Amaru, 2007), PRI-P05 (Montelli et al., 2006), and LLNL_G3Dv3 (Simmons et al., 2012). UU-P07 was computed using P-wave travel time data and a global surface-wave model as a reference, which provides a more realistic lithospheric structure than most teleseismic body-wave models. PRI-P05 is a finite-frequency P-wave model based on the arrival times of P-waves. LLNL_G3Dv3 is a global P-wave velocity model computed with 3-D ray tracing. The three global S-wave models are SGLOBE-rani (Chang et al., 2015), S40RTS (Ritsema et al., 2011), and SEMUCB-WM1(French and Romanowicz, 2014). SGLOBE-rani is a global radially anisotropic shear wave speed model with radial anisotropy allowed in the whole mantle. S40RTS is a global S-wave velocity model from Rayleigh wave dispersion, teleseismic traveltime, and normal-mode measurements. SEMUCB-WM1 is a whole-mantle radially anisotropic shear velocity structure obtained from spectral-element waveform tomography.

Comparison among these models is also useful to understand if this anomaly extends into the MTZ and lower mantle and is continuous down to the core-mantle boundary (CMB). Fig. 8 illustrates the velocity anomalies at 200 km depth and the same cross-section AA' as the regional model (Fig. 3) according to the six global models. Fig. 9 shows the velocity structure within the MTZ, at 500 km depth, and the cross-section DD' as that in *AF2019*.

Using different techniques and data to generate these images, some discrepancies between the models are expected. However, the large-scale features seen in the regional upper-mantle model can also be observed in the global P- and S-wave models, although our resolution is higher. All models show the high velocities below the Arabian Platform and Zagros Mountains, and lower velocities in the surrounding areas, but our images resolve greater details. More importantly, the tilted Levant anomaly in the upper mantle is detected in most of the models, especially in the P-wave images. UU-P07, PRI-P05, and SGLOBE-rani show that the Levant anomaly is continuous and extending through the MTZ, while the remaining global models image the same feature, but with a thin high-velocity anomaly separating the asthenospheric low-velocity body from that at the base of the MTZ and uppermost lower mantle.

The occurance of this anomaly in all the models confirms that this upper-mantle feature is robust, although it is unclear if it is detached from the source in the lower mantle or continuous. The whole-mantle models can also reveal how the Levant anomaly extends in the deeper mantle down to the CMB. The cross-sections AA' and DD' of all global models (Figs. 8 and 9) illuminate a prominent high-velocity anomaly in the mid-lowermost mantle (1200–2200 km depth). This fast (and cold)

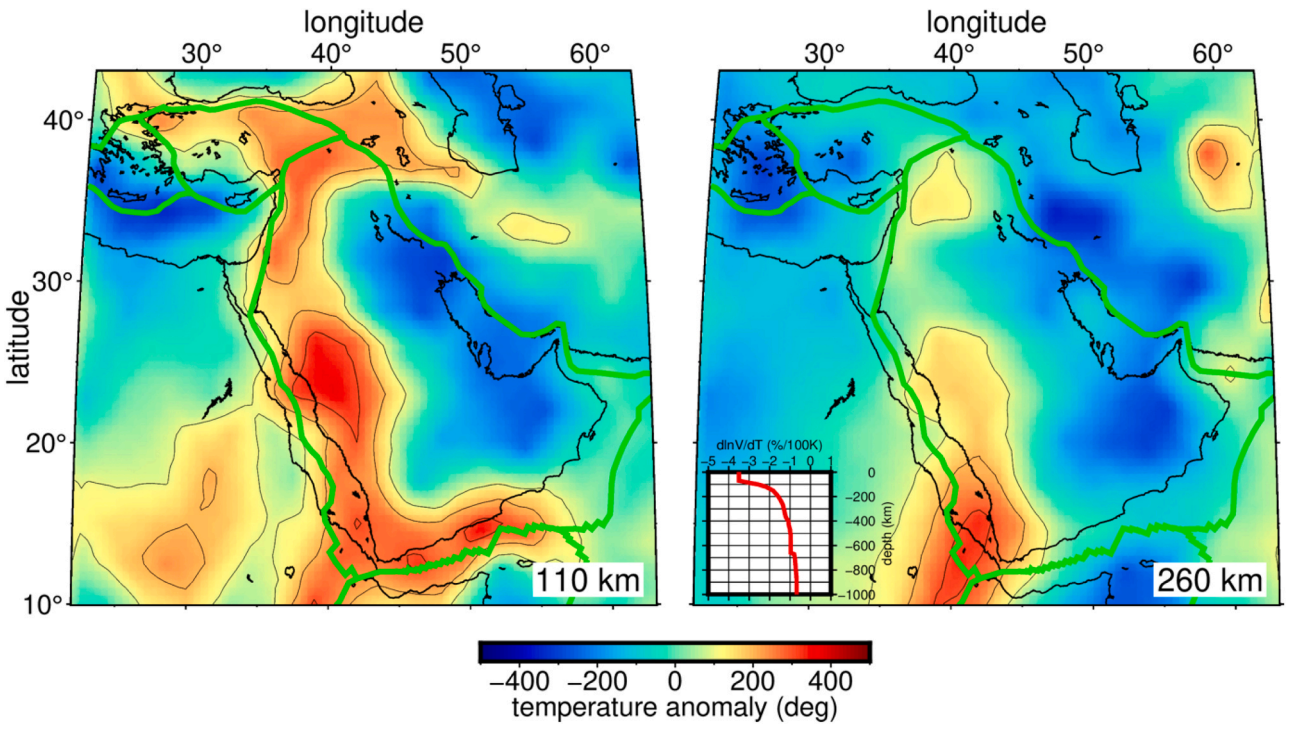

Fig. 7. Map views at 110- (left panel) and 260-km (right panel) depth, showing the thermal anomalies obtained from the conversion of the S-wave velocities to temperature anomalies using the dV_S/dT derivative of Styles et al. (2011). The spacing between the contours is 100 °C and is plotted only for the positive temperature anomalies. Inset: The red curve indicates the isomorphic (which does not consider the effects of phase-boundary topography) dV_S/dT derivative used to convert the low-velocity structure to temperature anomaly. For a continuous thermal upper mantle having 100–200 K excess temperature, we expect to see V_S anomalies of ~1% at the top of the MTZ, and ~1.5% at 200 km depth. Plate boundaries are shown as green lines.

body separates the Levant's low-velocity feature imaged in the upper mantle from another low-velocity anomaly located at the base of the mantle, which could be viewed as its deep source (Fig. 8). It also appears to be disconnected from the strong high-velocity anomaly in the upper mantle ascribed to the Arabian Platform (Fig. 9).

4. Residual topography

We also compute residual topography to provide insights into anomalous topography in the region (Fig. 10A). Residual topography (h_{res}) is commonly defined as the difference between the observed elevation (h) and the expected elevation based on the approximation for isostatic compensation of the crust ($H_c - H_o$; Gvirtzman and Nur, 2001):

$$h_{res} = h - (H_c - H_o)$$

$$H_c = \left(\frac{\rho_a - \rho_c}{\rho_a}\right) H$$

where H_c is the contribution of crustal buoyancy to surface topography, H is the crustal thickness, ρ_a is the density of the asthenosphere, and ρ_c is the density of the crust. H_o is a constant that reduces residuals to a reference level, and h_{res} represents the part of the topography/bathymetry that is not balanced by the crustal structure.

H_o is taken as 2.4 km, which is the mean value for mid-ocean ridge elevation (Lachenbruch and Morgan, 1990). We compile global databases as the input data—CRUST1.0 (Laske et al., 2013) for the crustal thickness and ETOPO2 (derived from the 2-min Gridded Global Relief Data Collection topography) for the topography—to investigate the regional effects of the residual topography in the MER (Fig. 10A). Densities are defined as $\rho_a = 3200$ kg m^{-3} and $\rho_c = 2840$ kg m^{-3}. As noted by Kounoudis et al. (2020), the residual topography expected from a 35 km-thick continental crust under isostatic equilibrium at zero elevation is defined as a common reference for Airy isostasy (Yu et al., 2016). For crustal buoyancy alone, this crustal value would lead to a negative residual topography of − 1.5 km, implying that a negatively buoyant, 96-km thick lithospheric mantle is required to keep the top of the crust at sea level. Following this simple approach, residuals greater than − 1.5 km show that the surface topography is higher than what would be expected assuming isostatic conditions and thus is in an undercompensated state, while in the opposite case, the crust is in an overcompensated state. This means that residual topography higher than − 1.5 km requires additional vertical support against the gravitation, which may be generated by mantle convection (McKenzie, 2010). Vice versa, lower values of residual topography implies a thicker mantle lithosphere and/or a downward pulling flow. The variations of residual topography are in general agreement with previous studies, especially considering the different approach used (Faccenna et al., 2014; Kaban et al., 2016a, 2016b; Komut et al., 2012; Kounoudis et al., 2020; Şengül Uluocak et al., 2021). However, in Kaban et al. (2016a) and (2016b) the residual topography is positive both in the Arabian Shield and Platform and becomes weakly positive along the SE margin of the Arabian plate. In contrast to the results of Kaban et al. (2016a), we find a large difference in the residual topography between the Arabian platform and Arabian Shield (Fig. 10). On the other hand, the estimates of Kaban et al. (2016a, 2016b) do not include the effect of the density variations related to the deep mantle, and, thus at least part of such difference may be associated with the removal of the deep signal. In more detail, we observe positive residual topography along the margins of the Gulf of Aden, in the Red Sea, and NE Ethiopia, with the absolute maximum over the Afar triple junction (+1 km, Fig. 10A), which is likely related to the hot mantle rising from deep depths. Slightly negative (values higher than −1.5 km) residual topography is found in Anatolia, Jordan, Syria, Lesser Caucasus, meaning that these regions deviate from Airy isostatic equilibrium and may call for other geodynamic mechanisms to keep elevated topography (i.e. buoyant deep material). Larger negative residuals are observed over the ZFTB and the southeastern Arabian

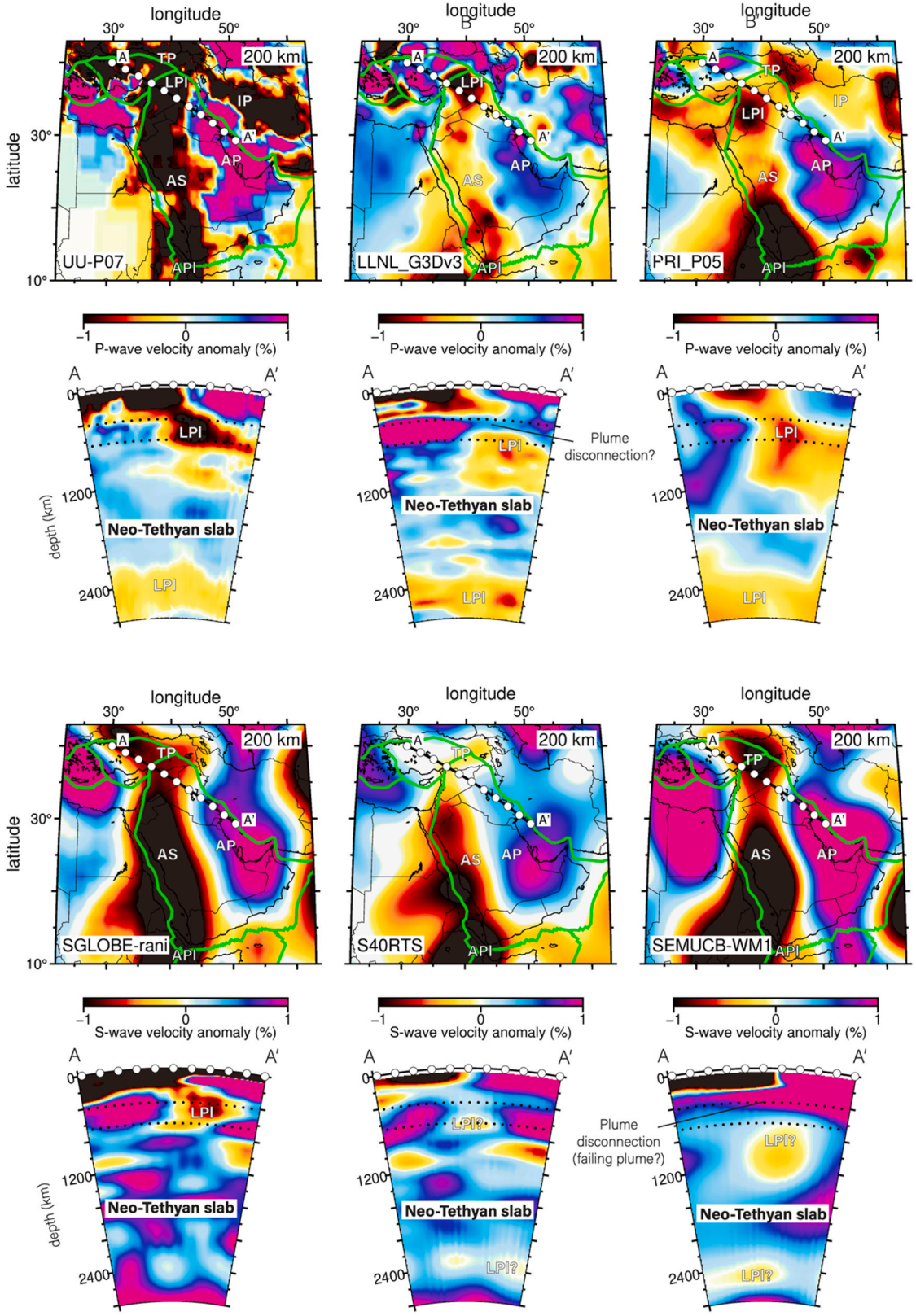

Fig. 8. Three global P- and three global S-wave models used to compare with our regional model and see the extension into the deep mantle of the upper-mantle anomalies. The P-wave models are shown in the first two rows: UU-P07 (Amaru, 2007), PRI-P05 (Montelli et al., 2006), and LLNL_G3Dv3 (Simmons et al., 2012). The S-wave models are plotted in the fourth and fifth rows: SGLOBE-rani (Chang et al., 2015), S40RTS (Ritsema et al., 2011), and SEMUCB-WM1 (French and Romanowicz, 2014). The map views are at 200 km depth. The cross-section AA' is the same as the regional waveform model in Fig. 3 and shows the tilted low-velocity anomaly in the upper mantle beneath the Levant and its continuation in the lower mantle cut by a prominent high-velocity body at mid-mantle depths interpreted as a remnant of the Neo-Tethyan slab. Plate boundaries in the map views are displayed as green lines. The MTZ discontinuities in the cross-sections are indicated with black points.

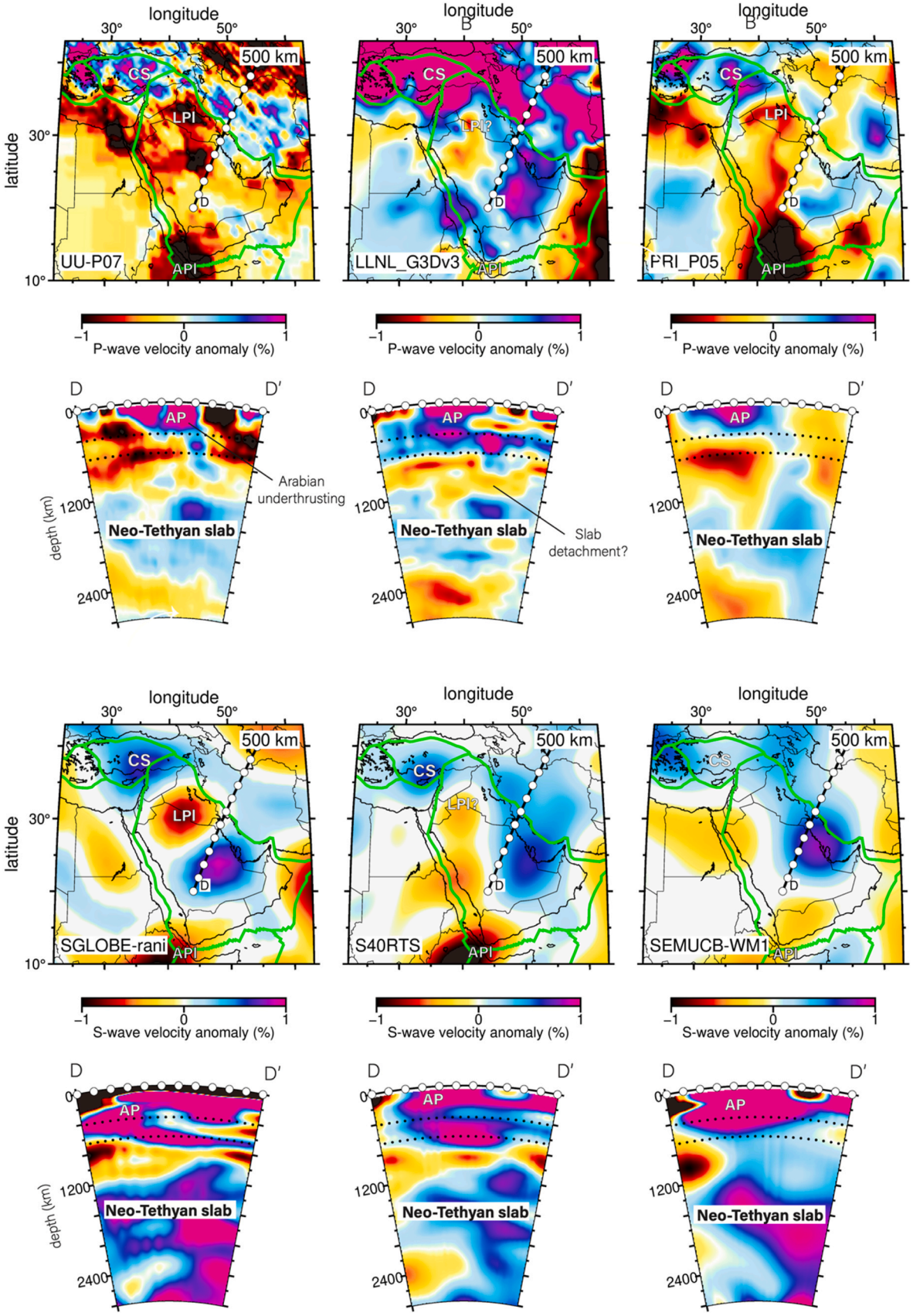

Fig. 9. Same as Fig. 8 but showing a different map view and cross-section. The map views are at 500 km depth, within the MTZ. The labels of the main features are the same as in Fig. 3. The cross-section DD' is the same as the model in Fig. 3 and shows the Arabian underthrusting beneath Iran and the piece of Neo-Tethyan slab sank in the lower mantle. Note that the two bodies appear detached just beneath the 660-km discontinuity.

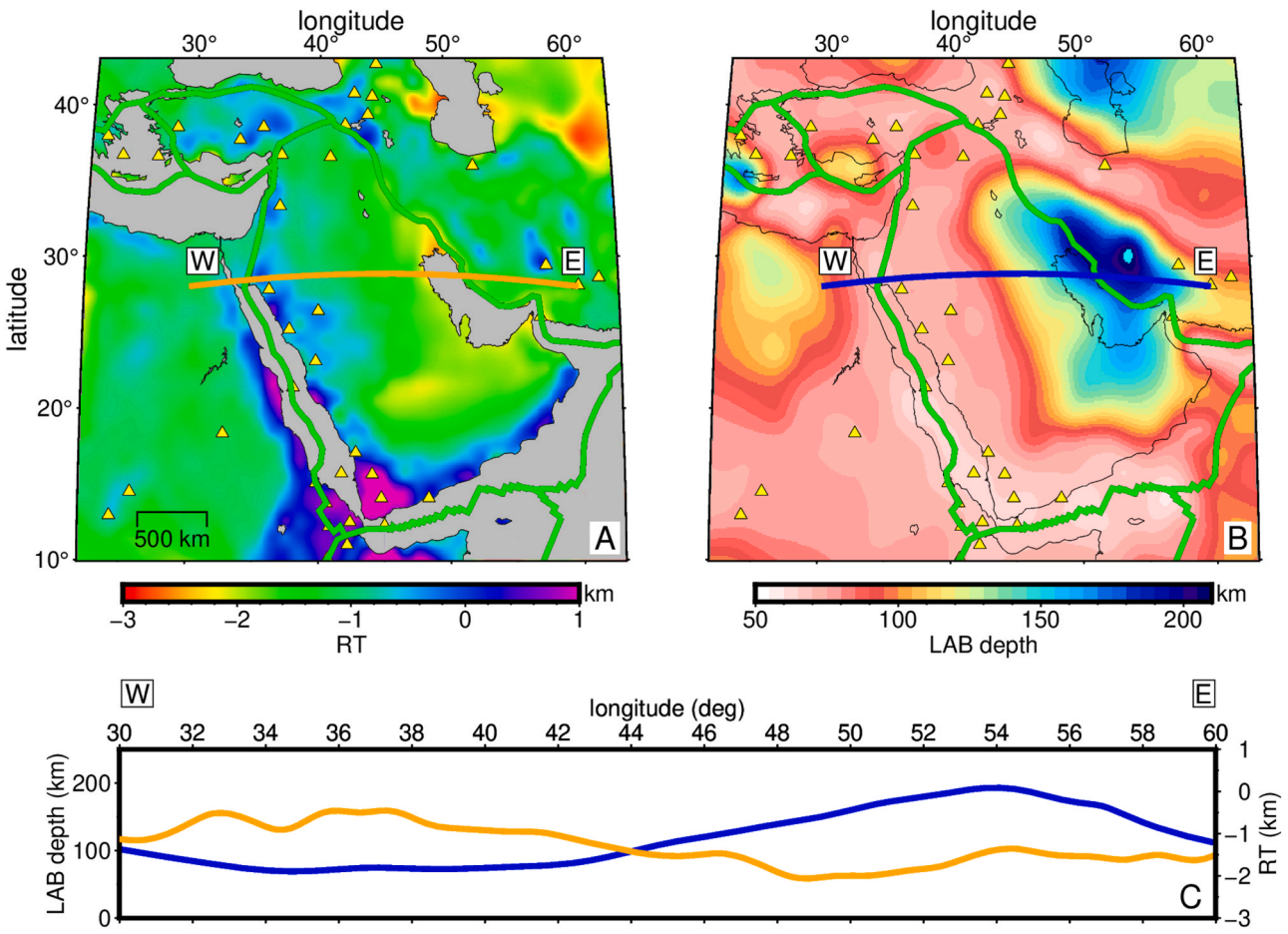

Fig. 10. A. Residual topography (RT) map of the MER computed using the crustal thickness of CRUST1.0 (Laske et al., 2013) and topography taken from ETOPO2 (https://doi.org/10.7289/V5J1012Q). B. Lithosphere-asthenosphere boundary (LAB) depth from the global WINTERC-G thermodynamic model of Fullea et al. (2021). Plate boundaries are displayed as green lines. C. W–E Profile through the Arabian Shield and Arabian Platform (orange line: RT; blue line: LAB depth). Note the overall consistency between the areas of anomalously high topography and those of lithospheric thinning, as well as of slow velocities and high temperatures in Figs. 3 and 7, respectively, and vice versa.

margin, likely due to the effect of the underlying thick and cold lithosphere. A negative residual topography is also found, surprisingly, in Central Iran (around –1.0–-1.4 km). This result may depend on the choice of the crustal thickness model and density values. Indeed, changing the crustal thickness or the density contrasts between the mantle lithosphere and crust impacts the result of the residual topographies. For example, by including the higher-resolution regional crustal model of Kaviani et al. (2020), based on Raleigh wave records obtained from ambient-noise cross-correlations and regional earthquakes, results in a small increment of the extent of positive residuals both in Anatolia and Iran (Fig. S1). Considering the large uncertainties that CRUST 1.0 model can have in areas poorly covered by seismic data, we also estimate the effect of varying its crustal thickness of ± 5 km (Fig. S2) and density of ± 30 kg m^{-3} on the residual topography estimates (Fig. S3). We observe that a decrease of 5 km in crustal thickness and an increase of 30 kg m^{-3} lead to a near-zero or slightly positive residual topography in both the Anatolian and Iranian Plateaus. Pronounced negative residual topography anomalies (up to −3 km) are also observed in the South Caspian basin and in Iraq.

Although with large-scale resolution, the recent global thermochemical model of the upper mantle WINTERC–G (Fullea et al., 2021) confirms that the continental lithosphere in this region has strong lateral variations of the lithosphere-asthenosphere boundary (LAB) depth (Fig. 10B) and shows a good correlation with the residual topography pattern (see the W–E profile in Fig. 10C). Overall, it pinpoints a significantly thin lithosphere in northern East Africa, western Arabia, Levant, and Anatolia showing a minimum LAB depth (50–70 km) below Afar, the Arabian Shield, and the Gulf of Aden, where the residual topography anomaly is high. In the adjacent areas, where the residual topography is negative, the lithosphere shows an increasing thickness moving from the Arabian Platform (130–170 km) to the Zagros Mountains (> 200 km).

5. XKS splitting measurements

Mantle deformation geometry can be investigated by measuring the orientation and magnitude of seismic azimuthal anisotropy (Babuska and Cara, 1991; Zhang and Karato, 1995). Splitting of P-to-S converted phases as PKS, SKKS, and SKS (collectively referred to as XKS) at the CMB is one of the most frequently used diagnostic tools to infer the lattice-preferred orientation (LPO) of anisotropic minerals in the Earth's crust and mantle (Fouch and Rondenay, 2006; Nicolas and Christensen, 2011; Savage, 1999; Wüstefeld et al., 2009). Olivine is the most abundant anisotropic mineral crystal in the upper mantle. The shear strain induced by the mantle flow field aligns the *a*-axis of olivine to be parallel to the current or past flow direction (i.e., in case there is a vertical gradient in flow velocity) or perpendicular to the direction of maximum compression (Mainprice et al., 2000; Silver and Chan, 1991).

Upper-mantle anisotropy can be due to both asthenospheric and lithospheric sources (Ribe, 1989). We expect anisotropy to actively form at asthenospheric depths as the viscous shear accommodates the differential movement between the rigid lithosphere and the upper mantle. The strength of the lithospheric rocks instead can resist any active

deformation due to the recent mantle flow. Hence, lithospheric anisotropy is generally not induced by present-day plate motions but it may contain fossil anisotropic fabric associated with past tectonic processes (Babuska and Cara, 1991; Long and Silver, 2009; Silver, 1996). When the contribution of fossil lithospheric anisotropy is small, seismic anisotropy can be interpreted as a measure of recent flow in the mantle and represents a possible indicator for mantle convection.

Several XKS splitting studies have been performed on the MER and the resulting measurements are ideal for interpreting anisotropy induced by asthenospheric flow, especially where a thick overlying lithosphere that may also contribute to the observed anisotropy is lacking. We collect the most up-to-date splitting results from many regional studies (Arvin et al., 2021; Gao et al., 2010; Kaviani et al., 2021; Paul et al., 2014; Qaysi et al., 2018) to provide a dataset of anisotropy observations, which we combine in our geophysical analysis for studying the geodynamics of our region of interest. In Fig. 11, we show the compilation of splitting observations plotted on top of the regional waveform tomography model at 110 km depth. Overall, we observe a relatively uniform NE–SW oriented azimuthal anisotropy in the northern Arabian Shield, Anatolia, NW Iran, and part of the Zagros; on the contrary, anisotropy shows a more heterogenous pattern across the Arabian Platform and the Iranian Plateau with many local-scale variations including an N–S trend in eastern Iran, a NW–SW trend at the boundary between the Zagros and Central Iran, and a W–E trend in the Gulf of Aden.

Beneath the Arabian Shield, the model images an elongated low-velocity channel in the uppermost mantle, where the fast directions exhibit N–S to NE–SW orientations (Fig. 11). This orientation is kept also in Ethiopia around the Afar hotspot. In the adjacent high-velocity Arabian Platform, the anisotropic trend is more complex, without a dominant pattern of fast velocity directions. Only in its eastern part, the anisotropy is mostly trending NE–SW.

Moving to the north, the fast velocity directions keep a NE–SW orientation both in Anatolia, Levant (despite a significant lack of data around Syria and Iraq), and northern Iran although a thin NW-oriented bend in the fast-propagation direction is observed in the Iranian Plateau and at the boundary between the Zagros and Central Iran.

Assuming that the anisotropy comes from a low-viscosity asthenosphere, we can use this compilation together with other geophysical and geological information to assess the direction of the mantle flow (Becker et al., 2003; Silver and Holt, 2002).

6. Discussion

Interaction among different geological features, forming a complex tectonic system such as the MER can significantly affect the mantle flow field. The role of active asthenospheric mantle processes is still an open question mainly because of the lack of a comprehensive analysis of the velocity structures in relation to the surface, lithospheric, and deep mantle processes. In order to investigate the impact of mantle dynamics on the tectonic evolution of the region and, in particular, to address the issue of the interaction of mantle upwelling with the lithosphere, we compare the observed fast orientations of anisotropy with seismic tomography and other geophysical data. The integration of different sources of data suggests that two sub-vertical low-velocity anomalies in Afar and Levant –interpreted as active, warm mantle plumes– induce horizontal mantle flow exerting basal shear tractions on plates. Below we explain how such upwelling-induced tractions represent the primary driving forces for the plate motions in the region.

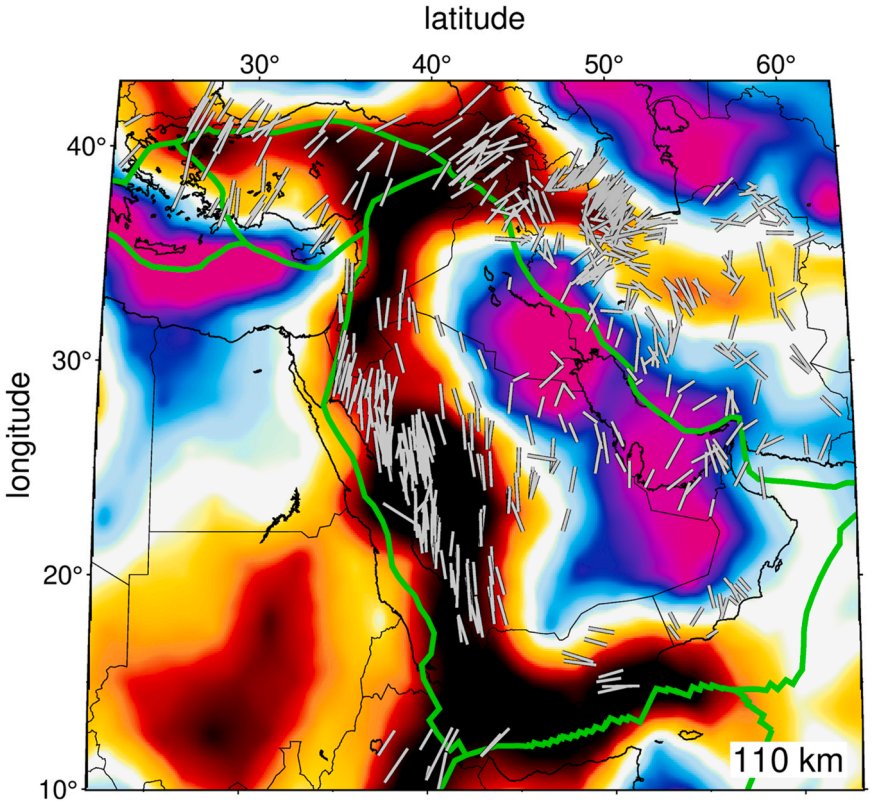

Fig. 11. Map of the integrated XKS splitting measurements (grey bars) for the MER plotted on top of the regional tomography model at 110 km depth. The splitting measurements are compiled from previous anisotropy studies (Arvin et al., 2021; Gao et al., 2010; Kaviani et al., 2021; Paul et al., 2014; Qaysi et al., 2018). The anisotropic fast-propagation directions are predominantly NE–SW oriented and indicate the horizontal mantle flow sourced by the two plumes of the region (the Afar and Levant Plumes) within the thin-lithosphere corridors in W Arabia, Levant, Anatolia, and NW Iran. Plate boundaries are displayed as green lines.

6.1. Large-scale mantle flow beneath the MER driven by the Afar and Levant Plumes

The mapping of splitting patterns in Fig. 11 indicates that the fast-propagation direction is NNE–oriented over most of Arabia and shows the same orientation as that in East Africa (e.g., Bagley and Nyblade, 2013; Elsheikh, 2019; Gao et al., 2010; Gashawbeza et al., 2004; Hammond et al., 2014; Kendall et al., 2006). Seismic velocities and their conversion to temperature anomalies suggest that the upper mantle beneath western Arabia is slow compared to the adjacent Arabian Platform and significantly warm (up to 300 °C temperature excess). In agreement with previous studies (Biryol et al., 2010; Chang and Van der Lee, 2011; Gao et al., 2010; Paul et al., 2014; Wolfe et al., 1999), we believe that this simple and relatively coherent anisotropic trend is mainly caused by the asthenospheric flow. The horizontal component of this flow is generated by the Afar Plume, which impinged the lithosphere ~40 Ma –at the time when the rapid Arabia motion started– and channelized beneath areas of thinned lithosphere progressively feeding the Cenozoic magmatic fields found in the Arabian Shield (the Arabian 'harrats'). This hypothesis is also consistent with the presence of a positive residual topography in western Arabia (Fig. 10), which points out the need for a thermal heterogeneity within the upper mantle to support the anomalously high topography. The localized W–E trend of anisotropy observed in the Gulf of Aden is ascribed to a branch of the Afar mantle plume head (see the elongated low-velocity anomaly propagating eastward from Afar), which spreads beneath the thinned lithosphere of the Aden rift (Civiero et al., 2022).

In the Levant region, the tilted low-velocity anomaly found below Iraq and Syria provides evidence for another localized mantle upwelling –the Levant Plume– which appears detached from its deep source at the CMB. As shown by the whole-mantle seismic tomography models in Fig. 8, a positive velocity anomaly cuts the Levant anomaly reaching the lower depths of the mantle. This broad high-velocity body has been interpreted as the remnant of the detached branch of the Neo-Tethyan slab –called the Mesopotamian slab– which may have interrupted the continuity of this deep-seated plume (van der Meer et al., 2018). Hafkenscheid et al. (2006) predicted the present positions of Neo-Tethyan lithospheric domains subducted, since the Mesozoic using a global mantle P-wave tomography model and found that most of the subducted Neo-Tethyan lithosphere is currently in the lower mantle between 800 and 2000 km depth. According to the kinematic model by Müller et al. (2008), it has been inferred that the subduction of this part of Neo-Tethys started ~165 Ma and ceased at approximately 79 Ma (Butterworth et al., 2014). A recent thermo-dynamic model also demonstrates that the slab folded at the MTZ before penetrating the lower mantle (Boutoux et al., 2021).

The regional *AF2019* model shows that the uppermost mantle region of slow velocities beneath the Levant connects with the low-velocity corridor in western Arabia and extends east towards Anatolia. Splitting measurements around this area are still predominantly NE–SW-oriented and the topography is anomalously high giving rise to the Anatolian Plateau. Moreover, as evidenced by Civiero et al. (2022), the volcanism at most locations has continued until the present and propagates more than a thousand of kilometers away toward Anatolia. These observations lead us to propose that an additional mantle source represented by the Levant Plume may be required to explain these phenomena at the surface. According to our interpretation, the actively deforming mantle flows northward from the Afar hotspot and joins the hot material from the deflected Levant upwelling expanding further east beneath the thin Anatolian lithosphere.

Several numerical models simulated how the mantle convection associated with mantle upwelling interacts with plate tectonics and dynamic topography in Africa and the MER (e.g., Becker and Faccenna, 2011; Behn et al., 2004; Conrad and Behn, 2010; Daradich et al., 2003; Faccenna et al., 2013; Forte et al., 2010; Moucha and Forte, 2011). Although using different approaches, they found that the viscous mantle flow is induced by a deep-seated broad upwelling beneath South Africa –the African Superplume. Recently, McKenzie (2020) has argued that the topography of the MER with wavelengths longer than 300 km results from mantle convection in the form of lines of rising material, which link multiple plumes. These upwellings generate magmas at depths of 60–80 km with a composition controlled by that of the convecting upper mantle. This scenario is consistent with our combined geophysical observations, which provide evidence that the mantle flow field is not driven by the large African Superplume rising to the upper mantle and directly impinging at the base of the lithosphere but by smaller-scale upper-mantle plumes localized in different parts of our study region. The deep origin of such small-scale upper mantle upwellings is still controversial (especially for the Afar Plume) and some studies do not observe a direct connection with the lower-mantle African Superplume (Boyce et al., 2021; Chang et al., 2020; Civiero et al., 2022; Tsekhmistrenko et al., 2021). For example, according to a recent 'vote analysis' involving 34 whole-mantle tomography models, two scenarios –one involving a single source located offshore Somalia and another one invoking two distinct sources in the lowermost mantle right beneath them and both perturbed by the Neo-Tethyan slab– have been proposed as alternative hypotheses (Civiero et al., 2022).

The relatively rapid plateau uplift (2 km since ~20 Ma), lithospheric thinning, and active volcanism observed in Anatolia have been often explained by mantle upwelling in response to lithospheric delamination (Bartol and Govers, 2014; Göğüş et al., 2017; Göğüş and Psyklywec, 2008), slab breakoff and tearing (Confal et al., 2020; Keskin, 2003; Menant et al., 2016; Rabayrol et al., 2019; Şengör et al., 2003), dripping/foundering of continental lithosphere (Kounoudis et al., 2020; Reid et al., 2019) and a regional mantle plume (Nikogosian et al., 2018). The Anatolian block also shows predominantly shallow and diffuse seismicity, indicating that the crust is still being actively deformed (Fig. 2A). Le Pichon and Kreemer (2010), in agreement with the models of Faccenna et al. (2006) and Şengör et al. (2003), combined two geodynamic mechanisms proposing that the east Anatolian asthenospheric rise was initiated because of the detachment of the Hellenic-Cyprus subduction zone, which enabled the rollback-induced toroidal asthenospheric flow to its edges.

According to our S-wave tomography model, fast and slow velocities are imaged next to each other in the shallow asthenosphere beneath the Hellenic-Cyprus subduction system (Figs. 3 and 4). The lack of a high-velocity slab-related body below the eastern Cyprus domain and further east below Bitlis can represent a slab window (due to a breakoff) or an absence of subduction. In agreement with previous tomography models using body waves (Biryol et al., 2011; Kounoudis et al., 2020; Piromallo and Morelli, 2003; Portner et al., 2018; Wei et al., 2019) and surface waves (Salaün et al., 2012), we provide further evidence that the slab is not continuous and speculate that the opening of the slab window may have channelled the mantle flow arriving from the Levant and Arabia beneath this region. Within this system, the rolling-back Hellenic subduction, accelerated by the pull furnished laterally by the detached portion of the slab, may represent an extra force that produces mantle suction further favoring the lateral escape of Anatolia towards the retreating trench well documented by the GPS compilation (Fig. 2B).

It has been previously proposed that mantle drag, due to a large-scale convection cell, could efficiently push continental plates, thus facilitating collision (Alvarez, 2010; Sternai et al., 2014) and lateral escape (Becker and Faccenna, 2011; Van Benthem and Govers, 2010). Following this idea, we propose an updated geodynamic scenario, in which the horizontal traction of the mantle flow, induced by both the Afar and Levant Plumes, accelerates the Arabian plate motion to converge toward north and drags the lateral escape of Anatolia.

6.2. Combined plume- and slab-induced flow around the Zagros collision zone

The new, high-resolution images of the Zagros upper mantle allow us

to examine better the mantle dynamics around this collision zone. The NE–dipping high-velocity anomaly imaged beneath eastern Arabia (Figs. 3 and 4) associated with the lithospheric thickening (Fig. 10, Mohammadi et al., 2022; Priestley et al., 2012) clearly suggests that the Arabian passive margin (Arabian plate front) underthrusted beneath Iran, with a consequent strong deformation and thickening of the Arabian lithosphere during the collision. In line with this interpretation, a recent thermochemical modelling study has found that the lower part of the lithosphere in the Arabian plate is $\sim+25$ kg m^{-3} denser than the sub-lithospheric mantle, allowing underthrusting of the Arabian lithosphere beneath the Iranian Plateau (Mousavi et al., 2023). P and S receiver functions (Mohammadi et al., 2013; Motaghi et al., 2017; Paul et al., 2010, 2006) and ambient-noise images (Irandoust et al., 2022; Kaviani et al., 2020; Movaghari et al., 2021) also revealed a strong velocity contrast with a low dip to the northeast following the Main Zagros Thrust at the surface. This interface has been interpreted as the lithospheric-scale underthrusting of the Arabian slab beneath Central Iran.

Numerous investigations discuss whether such Arabian lithospheric slab is connected to the subducted Neo-Tethys oceanic lithosphere (see review of Agard et al., 2011). For example, many teleseismic tomography studies (Kaviani et al., 2007; Lei and Zhao, 2007; Rahmani et al., 2019; Shomali et al., 2011; Veisi et al., 2021; Zor, 2008) show low velocities just beneath the lithosphere and fast velocities in the MTZ beneath the Iranian Plateau. They concluded that the high-velocity anomaly beneath the Iranian Plateau is wholly separated from the Zagros lithosphere and can be interpreted as a remnant of the detached Tethyan slab, which results in a mantle upwelling (and lithospheric thinning) beneath Central Iran. Geochemical (Chiu et al., 2013; Omrani et al., 2008; Pang et al., 2013) and thermomechanical (Dymkova et al., 2016; François et al., 2014) studies suggested that the uplift and widespread Cenozoic calc-alkaline magmatism in eastern-central Iran was triggered by an upwelling process, which resulted from the weakening and convective removal of the thickened lithosphere after the collision. The seismological observations presented here (see, in particular, the cross-sections CC' and DD' in Fig. 4) do not reveal a discontinuity of the subducting high-velocity anomaly at asthenospheric depths and seem at odds with the proposed slab breakoff of continent-ocean transitional lithosphere in the upper mantle beneath the Zagros Mountains. However, since we do not have resolution below the MTZ, it could be that a slab breakoff occurred at deeper depths. The upper-mantle velocity structure teleseismically imaged by Mahmoodabadi et al. (2020, 2019) suggests that such breakoff would separate the Neo-Tethyan oceanic slab from the continental leading lithosphere. This agrees well with the global whole-mantle images of the 'Atlas of the underworld' (Agard et al., 2011; van der Meer et al., 2018) and with those displayed in Fig. 9 illustrating a thin low-velocity layer just below the base of the MTZ, which splits the underthrust Arabian Platform from the Neo-Tethyan oceanic piece of slab descending into the lower mantle.

The Zagros orogen is located between the oceanic subduction of Makran, eastern Anatolia, and the Alborz belt, where seismic analyses using receiver function (e.g., Mohammadi et al., 2013; Şengör et al., 2003; Wu et al., 2021; Zor et al., 2003), Pn phase (Al-Lazki et al., 2004, 2003; Barazangi et al., 2006) and surface-wave data (e.g., Mortezanejad et al., 2019; Priestley et al., 2012) suggested that the lithospheric mantle is either thinned or completely removed. The anisotropy field reveals a quite uniform NE–SW direction of the XKS splitting signal in NW Iran, which trends sub-parallel to the absolute plate motion vectors (N39°E). Arvin et al. (2021) concluded that the shearing at the base of the lithosphere may cause olivine LPO fabric in the asthenospheric mantle, while other authors (e.g., Sadeghi-Bagherabadi et al., 2018; Sadidkhouy et al., 2008) contended a purely asthenospheric origin due to mantle flow beneath the thinner lithosphere. Following our integrated geophysical analysis, we propose that the main driver of the mantle deformation is the hot mantle material coming from both the Afar and Levant Plumes, which has been channelized below the thin-lithosphere corridor below western Arabia and tilts laterally around the edge of the Arabian slab beneath the Zagros Mountains. Thus, the asthenospheric low-velocity anomaly observed beneath the Iranian Plateau can be the result of more than one contribution: i) a mantle rise in response to a breakoff of the oceanic Neo-Tethyan slab beneath Central Iran; and ii) the warm mantle flow coming laterally, as suggested by our findings. The mostly N–S oriented anisotropy in the eastern part of Iran is sub-parallel to the strike-slip zones (see Fig. 2A) meaning that the fault system here likely affects the entire lithosphere developing pervasive anisotropy (Gao et al., 2023; Kaviani et al., 2021).

Subduction- and keel-induced mantle circulation plays an important role in the dynamics of convergent margins. Kaviani et al. (2021) proposed that the pattern of azimuthal anisotropy observed around Zagros is mostly due to a circular flow component related to the thick lithospheric keel associated with the Arabian Platform. Several numerical and analog experiments (e.g., Funiciello et al., 2006; Király et al., 2017; Li and Ribe, 2012; Miller and Becker, 2012; Piromallo et al., 2006; Strak and Schellart, 2014) demonstrated that the convective flow field can be deflected by subducted slabs and cratonic keels. We indeed believe that part of this signal may be due to the lateral toroidal flow from behind the Arabian subducted slab around its edges where the lithosphere is thinner and less deformed. The prevalent NE-directed anisotropy reflects the part of the mantle flow lateral to the edges of the slab, while the NW-oriented pattern in front of it can indicate the tilting of the flow around the strong subducted lithosphere.

In sum, our tomography model combined with the measurements of seismic anisotropy clearly indicates that large-scale mantle flow exists from northeast Africa to the collision region of Eurasia, Arabia, and Anatolia. In Fig. 12 we show the direction of the mantle flow around the thick and cold lithosphere of the Arabian Platform and subduction slabs in a 3D projection of the *AF2019* tomography model using an indicative $\pm$ 1.9% contour for both the positive and negative velocity anomalies. The warm mantle rising from the vertical Afar plume channels horizontally beneath the thin lithospheric corridor of the Arabian Shield and merges with the material from the tilted Levant upwelling below Syria. At these latitudes, the low-viscosity mantle material bifurcates with a NE–SW component flowing around the edge of the cold Arabian slab and Caucasus Mountains and the other component eastwards beneath Anatolia, which is moving rapidly westward (Fig. 12A-B). In Anatolia, the GPS observations provide strong evidence for the vertically coherent deformation of the lithosphere and the tomography images indicate that the added flow from the Levant upwelling contributes significantly to the counterclockwise rotation of the plate. In addition, the detached Cyprus slab (Fig. 12C) may play a role in deflecting asthenospheric flow beneath the region. To the east, the hot plume-driven mantle material is added to the toroidal flow, which turns around the Arabian slab and emerges to the top side of it below the Iranian Plateau (Fig. 12D). The combination of the plume-driven and subduction-driven toroidal flow explains the dominant plate motion-parallel NE–SW anisotropy pattern and supports models of collision areas close to regions of mantle upwelling.

7. Conclusions

Based on an integration of different sources of observations coming from seismic tomography, anisotropy, and other geophysical and geological data, we propose an updated geodynamic scenario for the tectonic evolution of the Middle East region. Two low seismic velocity anomalies in the upper to lower mantle beneath northern East Africa and the Levant are robust features of both regional and global tomographic models. Assuming that the low velocities are due to warm, low-viscosity material, we ascribe such seismic anomalies to thermal upwellings, the Afar and Levant Plumes. These localized plumes, together with the slab pull exerted by the Hellenic-Cyprus subduction, affect the regional horizontal flow field in the uppermost mantle, which in turn facilitates the Arabia-Eurasia collision and the Anatolian westward plate motion.

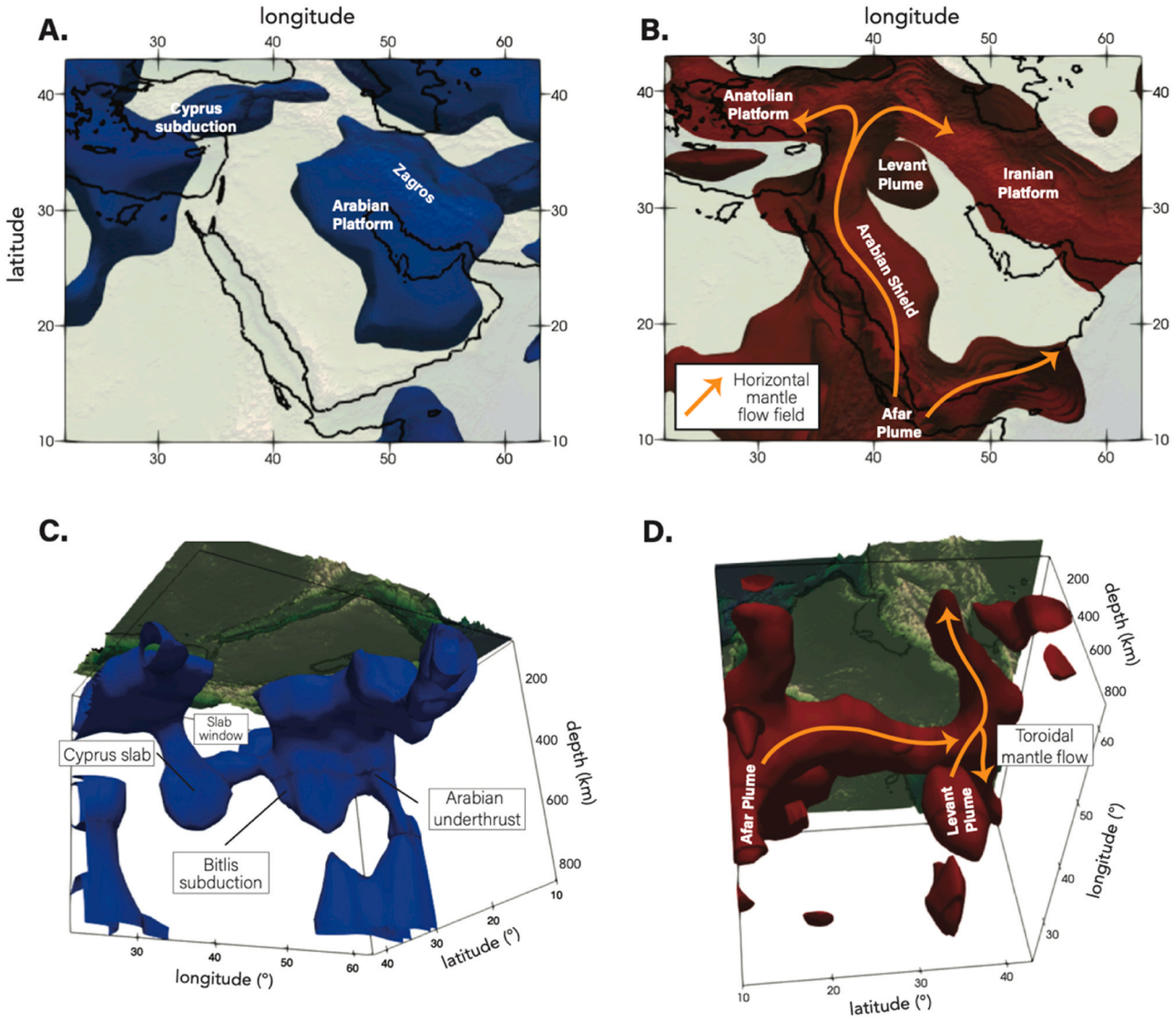

Fig. 12. 3D fast (in blue, panels A and C) and slow (in red, panels B and D) structure of the MER, displayed as velocity anomaly isosurfaces. Positive contours greater than 1.9% are shown in the 3D panel C. Negative contours lower than –1.9% are shown in the 3D panel D. Topography is displayed on top. Panels A and C favour the view of the subduction and relative slab windows; panels B and D illustrate the continuous channel of hot mantle material, flowing below the Arabian Shield, Levant, and around Zagros. The orange arrows indicate the directions of the horizontal mantle flow associated with the Afar (in the south) and Levant (in the north) plumes.

The plume-driven flow, combined with the toroidal forces associated with the Arabian slab, also influences the mantle circulation around the collision Zagros belt and the Iranian Plateau. Our synthesised results suggest a long-wavelength convective support of topography, which is also in agreement with the uncompensated pattern of residual topography and previous modelling studies. This large-scale mantle circulation flow has important implications for the geodynamics and geotectonics of the entire region and should be tested in future numerical experiments of mantle flow predictions.

CRediT authorship contribution statement

Civiero Chiara: Writing – original draft, Methodology, Funding acquisition, Formal analysis, Conceptualization. **Celli Nicolas Luca:** Software, Data curation. **Tesauro Magdala:** Writing – review & editing, Conceptualization.

Declaration of Competing Interest

The authors declare that they have no known competing financial interests or personal relationships that could have appeared to influence the work reported in this paper.

Data Availability

All data can bedowloaded freely or requested to the authors (it is a synthesis paper) and the link to the tomography model is specified in the manuscript.

Acknowledgments

We thank the Guest Editor Jaroslava Plomerova and two anonymous reviewers for valuable suggestions. We also thank Enrico Serpelloni and Lavinia Tunini for providing their GPS data compilations to plot in Fig. 2. All figures were created using Generic Mapping Tools (GMT; and Illustrator (https://adobe.com/products/illustrator). This work was supported by the grant CEX2019-000928-S funded by AEI 10.13039/501100011033. C. C. acknowledges the Programma Per Giovani Ricercatori "Rita Levi Montalcini" (grant D86-RALMI23CIVIE_01 awarded by the Italian Ministry of University and Research). M. T. acknowledges

funding from the Progress in Research of Interest (PRIN) project 2017: *Intraplate deformation, magmatism andtopographic evolution of a diffuse collisional belt: Insights into the geodynamics of the Arabia-Eurasia collisional zones*'.

Appendix A. Supporting information

Supplementary data associated with this article can be found in the online version at doi:10.1016/j.jog.2023.102005.

References

Agard, P., Omrani, J., Jolivet, L., Mouthereau, F., 2005. Convergence history across Zagros (Iran): Constraints from collisional and earlier deformation. Int. J. Earth Sci. 94, 401–419. https://doi.org/10.1007/s00531-005-0481-4.

Agard, P., Omrani, J., Jolivet, L., Whitechurch, H., Vrielynck, B., Spakman, W., Monié, P., Meyer, B., Wortel, R., 2011. Zagros orogeny: a subduction-dominated process. Geol. Mag. 148, 692–725. https://doi.org/10.1017/S001675681100046X.

Alinaghi, A., Koulakov, I., Thybo, H., 2007. Seismic tomographic imaging of P- and S-waves velocity perturbations in the upper mantle beneath Iran. Geophys. J. Int. 169, 1089–1102. https://doi.org/10.1111/j.1365-246X.2007.03317.x.

Al-Lazki, A.I., Seber, D., Sandvol, E., Turkelli, N., Mohamad, R., Barazangi, M., 2003. Tomographic Pn velocity and anisotropy structure beneath the Anatolian plateau (eastern Turkey) and the surrounding regions. Geophys. Res. Lett. 30, 4–7. https://doi.org/10.1029/2003GL017391.

Al-Lazki, A.I., Sandvol, E., Seber, D., Barazangi, M., Turkelli, N., Mohamad, R., 2004. Pn tomographic imaging of mantle lid velocity and anisotropy at the junction of the Arabian, Eurasian and African plates. Geophys. J. Int. 158, 1024–1040. https://doi.org/10.1111/j.1365-246X.2004.02355.x.

Alvarez, W., 2010. Protracted continental collisions argue for continental plates driven by basal traction. Earth Planet. Sci. Lett. 296, 434–442. https://doi.org/10.1016/j.epsl.2010.05.030.

Amaru, M.L., 2007. Global travel time tomography with 3-D reference models. Geol. Ultra 274, 174.

Amini, S., Shomali, Z.H., Koyi, H., Roberts, R.G., 2012. Tomographic upper-mantle velocity structure beneath the Iranian Plateau. Tectonophysics 554–557, 42–49. https://doi.org/10.1016/j.tecto.2012.06.009.

Artemieva, I.M., Mooney, W.D., 2002. On the relations between cratonic lithosphere thickness, plate motions, and basal drag. Tectonophysics 358, 211–231.

Arvin, S., Sobouti, F., Priestley, K., Ghods, A., Motaghi, K., Tilmann, F., Eken, T., 2021. Seismic anisotropy and mantle deformation in NW Iran inferred from splitting measurements of SK(K)S and direct S phases. Geophys. J. Int 226, 1417–1431. https://doi.org/10.1093/gji/ggab181.

Babuska, V., Cara, M., 1991. Seismic Anisotropy in the Earth. Springer Science & Business Media.

Bagley, B., Nyblade, A.A., 2013. Seismic anisotropy in eastern Africa, mantle flow, and the African superplume. Geophys. Res. Lett. 40, 1500–1505. https://doi.org/10.1002/grl.50315.

Balázs, A., Faccenna, C., Ueda, K., Funiciello, F., Boutoux, A., Blanc, E.J.P., Gerya, T., 2021. Oblique subduction and mantle flow control on upper plate deformation: 3D geodynamic modeling. Earth Planet. Sci. Lett. 569. https://doi.org/10.1016/j.epsl.2021.117056.

Barazangi, M., Sandvol, E., Seber, D., 2006. Structure and tectonic evolution of the Anatolian plateau in eastern Turkey.

Bartol, J., Govers, R., 2014. A single cause for uplift of the Central and Eastern Anatolian plateau. Tectonophysics 637, 116–136. https://doi.org/10.1016/j.tecto.2014.10.002.

Bastow, I.D., Nyblade, A.A., Stuart, G.W., Rooney, T.O., Benoit, M.H., 2008. Upper mantle seismic structure beneath the Ethiopian hot spot: Rifting at the edge of the African low-velocity anomaly. Geochem. Geophys. Geosystems 9, Q12022.

Becker, T.W., Faccenna, C., 2011. Mantle conveyor beneath the Tethyan collisional belt. Earth Planet. Sci. Lett. 310, 453–461. https://doi.org/10.1016/j.epsl.2011.08.021.

Becker, T.W., Kustowski, B., Ekström, G., 2008. Radial seismic anisotropy as a constraint for upper mantle rheology. Earth Planet. Sci. Lett. 267, 213–227. https://doi.org/10.1016/j.epsl.2007.11.038.

Becker, T.W., Lebedev, S., Long, M.D., 2012. On the relationship between azimuthal anisotropy from shear wave splitting and surface wave tomography. J. Geophys. Res. Solid Earth 117, 1–17. https://doi.org/10.1029/2011JB008705.

Becker, T.W., Kellogg, J.B., Ekström, G., O'connell, R.J., 2003. Comparison of azimuthal seismic anisotropy from surface waves and finite strain from global mantle-circulation models. Geophys. J. Int.

Behn, M.D., Conrad, C.P., Silver, P.G., 2004. Detection of upper mantle flow associated with the African Superplume. Earth Planet. Sci. Lett. 224, 259–274. https://doi.org/10.1016/j.epsl.2004.05.026.

Benoit, M.H., Nyblade, A.A., Owens, T.J., Stuart, G., 2006. Mantle transition zone structure and upper mantle S velocity variations beneath Ethiopia: Evidence for a broad, deep-seated thermal anomaly. Geochem. Geophys. Geosystems 7. https://doi.org/10.1029/2006GC001398.

Berberian, M., 1995. Master "blind" thrust faults hidden under the Zagros folds: active basement tectonics and surface morphotectonics. Tectonophysics 193–224.

Bercovici, D., Ricard, Y., Richards, M.A., 2000. The Relation Between Mantle Dynamics and Plate Tectonics: A Primer.

Biryol, B.C., Beck, S.L., Zandt, G., Özacar, A.A., 2011. Segmented African lithosphere beneath the Anatolian region inferred from teleseismic P-wave tomography. Geophys. J. Int. 184, 1037–1057. https://doi.org/10.1111/j.1365-246X.2010.04910.x.

Biryol, B.C., Zandt, G., Beck, S.L., Ozacar, A.A., Adiyaman, H.E., Gans, C.R., 2010. Shear wave splitting along a nascent plate boundary: the North Anatolian Fault Zone. Geophys. J. Int 181, 1201–1213. https://doi.org/10.1111/j.1365-246X.2010.04576.x.

Boutoux, A., Briaud, A., Faccenna, C., Ballato, P., Rossetti, F., Blanc, E., 2021. Slab Folding and Surface Deformation of the Iran Mobile Belt. Tectonics 40. https://doi.org/10.1029/2020TC006300.

Boyce, A., Bastow, I.D., Cottaar, S., Kounoudis, R., De Courbeville, J.G., Caunt, E., Desai, S., 2021. AFRP20: New P-wavespeed Model for the African Mantle Reveals Two Whole-Mantle Plumes Below East Africa and Neoproterozoic Modification of the Tanzania Craton. Geochem. Geophys. Geosystems 22 e2020GC009302.

Butterworth, N.P., Müller, R.D., Quevedo, L., O'Connor, J.M., Hoernle, K., Morra, G., 2014. Pacific plate slab pull and intraplate deformation in the early Cenozoic. Solid Earth 5, 757–777. https://doi.org/10.5194/se-5-757-2014.

Byrne, D.E., Sykes, L.R., Davis, D.M., 1992. Great thrust earthquakes and aseismic slip along the plate boundary of the Makran subduction zone. J. Geophys. Res 97, 449–478. https://doi.org/10.1029/91JB02165.

Cammarano, F., Goes, S., Vacher, P., Giardini, D., 2003. Inferring upper-mantle temperatures from seismic velocities. Phys. Earth Planet. Inter. 138, 197–222. https://doi.org/10.1016/S0031-9201(03)00156-0.

Celli, N.L., Lebedev, S., Schaeffer, A., Gaina, C., 2020. African cratonic lithosphere carved by mantle plumes. Nat. Commun. 11, 92. https://doi.org/10.1038/s41467-019-13871-2.

Chang, S., Kendall, E., Davaille, A., Ferreira, A.M.G., 2020. The evolution of mantle plumes in East Africa. J. Geophys. Res. Solid Earth 125. https://doi.org/10.1029/2020JB019929.

Chang, S.J., Van der Lee, S., 2011. Mantle plumes and associated flow beneath Arabia and East Africa. Earth Planet. Sci. Lett. 302, 448–454. https://doi.org/10.1016/j.epsl.2010.12.050.

Chang, S.J., Merino, M., Van Der Lee, S., Stein, S., Stein, C.A., 2011. Mantle flow beneath Arabia offset from the opening Red Sea. Geophys. Res. Lett. 38, 1–5. https://doi.org/10.1029/2010GL045852.

Chang, S.J., Ferreira, A.M.G., Ritsema, J., Heijst, H.J., Woodhouse, J.H., 2015. Joint inversion for global isotropic and radially anisotropic mantle structure including crustal thickness perturbations. J. Geophys. Res. Solid Earth 120, 4278–4300. https://doi.org/10.1002/2014JB011824.Received.

Chang, S.J., Van Der Lee, S., Flanagan, M.P., Bedle, H., Marone, F., Matzel, E.M., Pasyanos, M.E., Rodgers, A.J., Romanowicz, B., Schmid, C., 2010. Joint inversion for three-dimensional S velocity mantle structure along the Tethyan. Margin J. Geophys. Res. Solid Earth 115, 1–22. https://doi.org/10.1029/2009JB007204.

Chiu, H.-Y., Chung, S.-L., Zarrinkoub, M.H., Mohammadi, S.S., Khatib, M.M., Iizuka, Y., 2013. Zircon U–Pb age constraints from Iran on the magmatic evolution related to Neotethyan subduction and Zagros orogeny. Lithos 162–163, 70–87. https://doi.org/10.1016/j.lithos.2013.01.006.

Chorowicz, J., 2005. The East African rift system. J. Afr. Earth Sci. 43, 379–410. https://doi.org/10.1016/j.jafrearsci.2005.07.019.

Civiero, C., Lebedev, S., Celli, N.L., 2022. A Complex Mantle Plume Head Below East Africa-Arabia Shaped by the Lithosphere-Asthenosphere Boundary Topography. Geochem., Geophys., Geosystems. https://doi.org/10.1029/2022GC010610.

Civiero, C., Armitage, J.J., Goes, S., Hammond, J.O.S., 2019a. The Seismic Signature of Upper-Mantle Plumes: Application to the Northern East African Rift. Geochem. Geophys. Geosystems 20, 6106–6122. https://doi.org/10.1029/2019GC008636.

Civiero, C., Custódio, S., Rawlinson, N., Strak, V., Silveira, G., Arroucau, P., Corela, C., 2019b. Thermal Nature of Mantle Upwellings Below the Ibero-Western Maghreb Region Inferred From Teleseismic Tomography. J. Geophys. Res. Solid Earth 124, 1781–1801. https://doi.org/10.1029/2018JB016531.

Civiero, C., Goes, S., Hammond, J.O.S., Fishwick, S., Ahmed, A., Ayele, A., Doubre, C., Goitom, B., Keir, D., Kendall, J.M., Leroy, S., Ogubazghi, G., Rümpker, G., Stuart, G. W., 2016. Small-scale thermal upwellings under the northern East African Rift from S travel time tomography. J. Geophys. Res. Solid Earth 2010, 1–14. https://doi.org/10.1002/2016JB013070.

Confal, J.M., Faccenda, M., Eken, T., Taymaz, T., 2018. Numerical simulation of 3-D mantle flow evolution in subduction zone environments in relation to seismic anisotropy beneath the eastern Mediterranean region. Earth Planet. Sci. Lett. 497, 50–61. https://doi.org/10.1016/j.epsl.2018.06.005.

Confal, J.M., Bezada, M.J., Eken, T., Faccenda, M., Saygin, E., Taymaz, T., 2020. Influence of Upper Mantle Anisotropy on Isotropic *P*- Wave Tomography Images Obtained in the Eastern Mediterranean Region. e2019JB018559 J. Geophys. Res. Solid Earth 125. https://doi.org/10.1029/2019JB018559.

Conrad, C.P., Behn, M.D., 2010. Constraints on lithosphere net rotation and asthenospheric viscosity from global mantle flow models and seismic anisotropy. Geochem. Geophys. Geosystems 11. https://doi.org/10.1029/2009GC002970.

Conrad, C.P., Behn, M.D., Silver, P.G., 2007. Global mantle flow and the development of seismic anisotropy: Differences between the oceanic and continental upper mantle. J. Geophys. Res. Solid Earth 112. https://doi.org/10.1029/2006JB004608.

Daradich, A., Mitrovica, J.X., Pysklywec, R.N., Willett, S.D., Forte, A.M., 2003. Mantle flow, dynamic topography, and rift-flank uplift of Arabia. Geology 31, 901–904. https://doi.org/10.1130/G19661.1.

Deschamps, F., Trampert, J., 2003. Mantle tomography and its relation to temperature and composition. Phys. Earth Planet. Inter. 140, 277–291. https://doi.org/10.1016/j.pepi.2003.09.004.

Di Giacomo, D., Robert Engdahl, E., Storchak, D.A., 2018. The ISC-GEM Earthquake Catalogue (1904-2014): Status after the Extension Project. Earth Syst. Sci. Data 10, 1877–1899. https://doi.org/10.5194/essd-10-1877-2018.
Dymkova, D., Gerya, T., Burg, J.-P., 2016. 2D thermomechanical modelling of continent–arc–continent collision. Gondwana Res 32, 138–150. https://doi.org/10.1016/j.gr.2015.02.012.
Ebinger, C., Sleep, N.H., 1998. Cenozoic magmatism throughout east Africa resulting from impact of a single plume. Nature 395, 788–791.
El-Sharkawy, A., Meier, T., Hübscher, C., Lebedev, S., Dannowski, A., Kopp, H., Behrmann, J.H., McGrandle, A., Hamada, M., 2021. Lithospheric structure of the eastern Mediterranean Sea: Inferences from surface wave tomography and stochastic inversions constrained by wide-angle refraction measurements. Tectonophysics 821, 229159. https://doi.org/10.1016/j.tecto.2021.229159.
Elsheikh, A.A., 2019. Seismic anisotropy and mantle flow beneath East Africa and Arabia. J. Afr. Earth Sci. 149, 97–108. https://doi.org/10.1016/j.jafrearsci.2018.08.002.
Faccenna, C., Becker, T.W., 2010. Shaping mobile belts by small-scale convection. Nature 465, 602–605. https://doi.org/10.1038/nature09064.
Faccenna, C., Becker, T.W., Jolivet, L., Keskin, M., 2013. Mantle convection in the Middle East: Reconciling Afar upwelling, Arabia indentation and Aegean trench rollback. Earth Planet. Sci. Lett. 375, 254–269. https://doi.org/10.1016/j.epsl.2013.05.043.
Faccenna, C., Bellier, O., Martinod, J., Piromallo, C., Regard, V., 2006. Slab detachment beneath eastern Anatolia: a possible cause for the formation of the North Anatolian fault. Earth Planet. Sci. Lett. 242, 85–97. https://doi.org/10.1016/j.epsl.2005.11.046.
Faccenna, C., Becker, T.W., Auer, L., Billi, A., Boschi, L., Brun, J.P., Capitanio, F.A., Funiciello, F., Horvàth, F., Jolivet, L., Piromallo, C., Royden, L., Rossetti, F., Serpelloni, E., 2014. Mantle dynamics in the Mediterranean. Rev. Geophys. 52, 283–332. https://doi.org/10.1002/2013RG000444.
Forte, A.M., Quéré, S., Moucha, R., Simmons, N.A., Grand, S.P., Mitrovica, J.X., Rowley, D.B., 2010. Joint seismic-geodynamic-mineral physical modelling of African geodynamics: a reconciliation of deep-mantle convection with surface geophysical constraints. Earth Planet. Sci. Lett. 295, 329–341. https://doi.org/10.1016/j.epsl.2010.03.017.
Fouch, M.J., Rondenay, S., 2006. Seismic anisotropy beneath stable continental interiors. Phys. Earth Planet. Inter. 158, 292–320. https://doi.org/10.1016/j.pepi.2006.03.024.
Fouch, M.J., Fischer, K.M., Parmentier, E.M., Wysession, M.E., Clarke, T.J., 2000. Shear wave splitting, continental keels, and patterns of mantle flow. J. Geophys. Res. Solid Earth 105, 6255–6275. https://doi.org/10.1029/1999jb900372.
François, T., Burov, E., Agard, P., Meyer, B., 2014. Buildup of a dynamically supported orogenic plateau: numerical modeling of the Zagros/Central Iran case study. Geochem. Geophys. Geosystems 15, 2632–2654. https://doi.org/10.1002/2013GC005223.
French, S.W., Romanowicz, B.A., 2014. Whole-mantle radially anisotropic shear velocity structure from spectral-element waveform tomography. Geophys. J. Int 199, 1303–1327. https://doi.org/10.1093/gji/ggu334.
Fullea, J., Lebedev, S., Martinec, Z., Celli, N.L., 2021. WINTERC-grav: mapping the upper mantle thermochemical heterogeneity from coupled geophysical-petrological inversion of seismic waveforms, heat flow, surface elevation and gravity satellite data. Geophys. J. Int. 226, 146–191.
Funiciello, F., Moroni, M., Piromallo, C., Faccenna, C., Cenedese, A., Bui, H.A., 2006. Mapping mantle flow during retreating subduction: Laboratory models analyzed by feature tracking. J. Geophys. Res. Solid Earth 111, 1–16. https://doi.org/10.1029/2005JB003792.
Gao, S.S., Liu, K.H., Abdelsalam, M.G., 2010. Seismic anisotropy beneath the Afar Depression and adjacent areas: Implications for mantle flow. J. Geophys. Res. Solid Earth 115, 1–15. https://doi.org/10.1029/2009JB007141.
Gao, Y., Chen, L., Yang, J., Wang, K., 2023. Rheological heterogeneities control the non-progressive uplift of the Young Iranian Plateau. Geophys. Res. Lett. 50. https://doi.org/10.1029/2022GL101829.
Gao, Y., Chen, L., Talebian, M., Wu, Z., Wang, X., Lan, H., Ai, Y., Jiang, M., Hou, G., Khatib, M.M., Xiao, W., Zhu, R., 2022. Nature and structural heterogeneities of the lithosphere control the continental deformation in the northeastern and eastern Iranian plateau as revealed by shear-wave splitting observations. Earth Planet. Sci. Lett. 578. https://doi.org/10.1016/j.epsl.2021.117284.
Gashawbeza, E.M., Klemperer, S.L., Nyblade, A.A., Walker, K.T., Keranen, K.M., 2004. Shear-wave splitting in Ethiopia: precambrian mantle anisotropy locally modified by Neogene rifting. Geophys. Res. Lett. 31, 2–5. https://doi.org/10.1029/2004GL020471.
Goes, S., Govers, R., Vacher, P., 2000. Shallow mantle temperatures under Europe from P and S wave tomography. J. Geophys. Res. 105, 11153–11169. https://doi.org/10.1029/1999jb900300.
Göğüş, O.H., Psyklywec, R.N., 2008. Mantle lithosphere delamination driving plateau uplift and synconvergent extension in eastern Anatolia. Geology 36, 723–726. https://doi.org/10.1130/G24982A.1.
Göğüş, O.H., Pysklywec, R.N., Şengör, A.M.C., Gün, E., 2017. Drip tectonics and the enigmatic uplift of the Central Anatolian Plateau. Nat. Commun. 8. https://doi.org/10.1038/s41467-017-01611-3.
Gök, R., Sandvol, E., Türkelli, N., Seber, D., Barazangi, M., 2003. Sn attenuation in the Anatolian and Iranian plateau and surrounding regions. Geophys. Res. Lett. 30. https://doi.org/10.1029/2003GL018020.
Gvirtzman, Z., Nur, A., 2001. Residual topography, lithospheric structure and sunken slabs in the central Mediterranean. Earth Planet. Sci. Lett. 187, 117–130.
Hafkenscheid, E., Wortel, M.J.R., Spakman, W., 2006. Subduction history of the Tethyan region derived from seismic tomography and tectonic reconstructions. J. Geophys. Res. Solid Earth 111. https://doi.org/10.1029/2005JB003791.
Hammond, J.O.S., Kendall, J.M., Wookey, J., Stuart, G.W., Keir, D., Ayele, A., 2014. Differentiating flow, melt, or fossil seismic anisotropy beneath Ethiopia. Geochem. Geophys. Geosystems 15, 1878–1894. https://doi.org/10.1002/2013GC005185.
Hammond, J.O.S., Kendall, J.M., Stuart, G.W., Ebinger, C.J., Bastow, I.D., Keir, D., Ayele, A., Belachew, M., Goitom, B., Ogubazghi, G., Wright, T.J., 2013. Mantle upwelling and initiation of rift segmentation beneath the Afar Depression. Geology 41, 635–638. https://doi.org/10.1130/G33925.1.
Hansen, S., Schwartz, S., Al-amri, A., Rodgers, A., 2006. Comb. plate Motion Density-driven Flow. asthenosphere Saudi Arab.: Evid. Shear-Wave Split. Seism. anisotropy 34, 869–872. https://doi.org/10.1130/G22713.1.
Hansen, S.E., Nyblade, A.A., 2013. The deep seismic structure of the Ethiopia/Afar hotspot and the African superplume. Geophys. J. Int 194, 118–124. https://doi.org/10.1093/gji/ggt116.
Hansen, S.E., Nyblade, A.A., Benoit, M.H., 2012. Mantle structure beneath Africa and Arabia from adaptively parameterized P-wave tomography: Implications for the origin of Cenozoic Afro-Arabian tectonism. Earth Planet. Sci. Lett. 319–320, 23–34. https://doi.org/10.1016/j.epsl.2011.12.023.
Hatzfeld, D., Molnar, P., 2010. Comparisons of the kinematics and deep structures of the Zagros and Himalaya and of the Iranian and Tibetan plateaus and geodynamic implications. Rev. Geophys. 48. https://doi.org/10.1029/2009RG000304.
Hearn, T.M., Ni, J.F., 1994. Pn velocities beneath continental collision zones: the Turkish-Iranian plateau. Geophys. J. Int. 117, 273–283. https://doi.org/10.1111/j.1365-246X.1994.tb03931.x.
Hempton, M.R., 1987. Constraints on Arabian Plate motion and extensional history of the Red Sea. Tectonics 6, 687–705. https://doi.org/10.1029/TC006i006p00687.
Holtzman, B.K., Kohlstedt, D.L., Zimmerman, M.E., Heidelbach, F., Hiraga, T., Hustoft, J., 2003. Melt Segregation and Strain Partitioning: Implications for Seismic Anisotropy and Mantle Flow. Science 301.
Irandoust, M.A., Priestley, K., Sobouti, F., 2022. High-resolution lithospheric structure of the zagros collision zone and Iranian Plateau. J. Geophys. Res. Solid Earth 127. https://doi.org/10.1029/2022JB025009.
Jackson, J., McKenzie, D., 1988. The relationship between plate motions and seismic moment tensors, and the rates of active deformation in the Mediterranean and Middle East. Geophys. J. 93, 45–73. https://doi.org/10.1111/j.1365-246X.1988.tb01387.x.
Kaban, M.K., El Khrepy, S., Al-Arifi, N., Tesauro, M., Stolk, W., 2016a. Three-dimensional density model of the upper mantle in the Middle East: Interaction of diverse tectonic processes. J. Geophys. Res. Solid Earth 121, 5349–5364. https://doi.org/10.1002/2015JB012755.
Kaban, M.K., Stolk, W., Tesauro, M., El Khrepy, S., Al-Arifi, N., Beekman, F., Cloetingh, S. A.P.L., 2016b. 3D density model of the upper mantle of Asia based on inversion of gravity and seismic tomography data. Geochem. Geophys. Geosystems 17, 4457–4477. https://doi.org/10.1002/2016GC006458.
Kaviani, A., Hatzfeld, D., Paul, A., Tatar, M., Priestley, K., 2009. Shear-wave splitting, lithospheric anisotropy, and mantle deformation beneath the Arabia-Eurasia collision zone in Iran. Earth Planet. Sci. Lett. 286, 371–378. https://doi.org/10.1016/j.epsl.2009.07.003.
Kaviani, A., Paul, A., Bourova, E., Hatzfeld, D., Pedersen, H., Mokhtari, M., 2007. A strong seismic velocity contrast in the shallow mantle across the Zagros collision zone (Iran). Geophys. J. Int 171, 399–410. https://doi.org/10.1111/j.1365-246X.2007.03535.x.
Kaviani, A., Sandvol, E., Moradi, A., Rümpker, G., Tang, Z., Mai, P.M., 2018. Mantle Transition Zone Thickness Beneath the Middle East: Evidence for Segmented Tethyan Slabs, Delaminated Lithosphere, and Lower Mantle Upwelling. J. Geophys. Res. Solid Earth 123, 4886–4905. https://doi.org/10.1029/2018JB015627.
Kaviani, A., Sandvol, E., Ku, W., Beck, S.L., Türkelli, N., Özacar, A.A., Delph, J.R., 2022. Seismic attenuation tomography of the Sn phase beneath the Turkish-Iranian Plateau and the Zagros mountain belt. Geosphere 18, 1377–1393. https://doi.org/10.1130/GES02503.1.
Kaviani, A., Mahmoodabadi, M., Rümpker, G., Pilia, S., Tatar, M., Nilfouroushan, F., Yamini-Fard, F., Moradi, A., Ali, M.Y., 2021. Mantle-flow diversion beneath the Iranian plateau induced by Zagros' lithospheric keel. Sci. Rep. 11. https://doi.org/10.1038/s41598-021-81541-9.
Kaviani, A., Paul, A., Moradi, A., Mai, P.M., Pilia, S., Boschi, L., Georg, R., Lu, Y., Tang, Z., Sandvol, E., 2020. OUP accepted manuscript. Geophys. J. Int. 1349–1365. https://doi.org/10.1093/gji/ggaa075.
Kendall, J.M., Pilidou, S., Keir, D., Bastow, I.D., Stuart, G.W., Ayele, A., 2006. Mantle upwellings, melt migration and the rifting of Africa: Insights from seismic anisotropy. Geol. Soc. Spec. Publ. 259, 55–72. https://doi.org/10.1144/GSL.SP.2006.259.01.06.
Keskin, M., 2003. Magma generation by slab steepening and breakoff beneath a subduction-accretion complex: An alternative model for collision-related volcanism in Eastern Anatolia, Turkey. Geophys. Res. Lett. 30, 7–10. https://doi.org/10.1029/2003GL018019.
Khorrami, F., Vernant, P., Masson, F., Nilfouroushan, F., Mousavi, Z., Nankali, H., Saadat, S.A., Walpersdorf, A., Hosseini, S., Tavakoli, P., Aghamohammadi, A., Alijanzade, M., 2019. An up-to-date crustal deformation map of Iran using integrated campaign-mode and permanent GPS velocities. Geophys. J. Int 217, 832–843. https://doi.org/10.1093/gji/ggz045.
Kim, R., Witek, M., Chang, S.-J., Lim, J.-A., Mai, P.M., Zahran, H., 2023. Isotropic and radially anisotropic S-velocity structure beneath the Arabian plate inferred from surface wave tomography. Tectonophysics 862, 229968. https://doi.org/10.1016/j.tecto.2023.229968.

Király, Á., Capitanio, F.A., Funiciello, F., Faccenna, C., 2017. Subduction induced mantle flow: Length-scales and orientation of the toroidal cell. Earth Planet. Sci. Lett. 479, 284–297. https://doi.org/10.1016/j.epsl.2017.09.017.
Komut, T., 2015. High surface topography related to upper mantle flow beneath Eastern Anatolia. Geophys. J. Int 203, 1263–1273. https://doi.org/10.1093/gji/ggv374.
Komut, T., Gray, R., Pysklywec, R., Göğüş, O.H., 2012. Mantle flow uplift of western Anatolia and the Aegean: Interpretations from geophysical analyses and geodynamic modeling. J. Geophys. Res. Solid Earth 117. https://doi.org/10.1029/2012JB009306.
Koulakov, I., Burov, E., Cloetingh, S., El Khrepy, S., Al-Arifi, N., Bushenkova, N., 2016. Evidence for anomalous mantle upwelling beneath the Arabian Platform from travel time tomography inversion. Tectonophysics 667, 176–188. https://doi.org/10.1016/j.tecto.2015.11.022.
Kounoudis, R., Bastow, I.D., Ogden, C.S., Goes, S., Jenkins, J., Grant, B., Braham, C., 2020. Seismic Tomographic Imaging of the Eastern Mediterranean Mantle: Implications for Terminal-Stage Subduction, the Uplift of Anatolia, and the Development of the North Anatolian Fault. Geochem. Geophys. Geosystems 21. https://doi.org/10.1029/2020GC009009.
Lachenbruch, A.H., Morgan, P., 1990. Continental extension, magmatism and elevation; formal relations and rules of thumb. Tectonophysics 174, 39.
Laske, G., Masters, G., Ma, Z., Pasyanos, M.E., 2013. CRUST1.0: an updated global model of earth's crust. Geophys Res Abstr. 15. Abstract EGU2013–2658.
Le Pichon, X., Kreemer, C., 2010. The miocene-to-present kinematic evolution of the eastern mediterranean and middle east and its implications for dynamics. Annu. Rev. Earth Planet. Sci. 38, 323–351. https://doi.org/10.1146/annurev-earth-040809-152419.
Le Pichon, X., Chamot-rooke, N., Noomen, R., 1995. Geodetic determination of the kinematics of central Greece with respect to Europe: Implications for eastern Mediterranean tectonics. J. Geophys. Res 100, 675–690.
Lees, M.E., Rudge, J.F., McKenzie, D., 2020. Gravity, Topography, and Melt Generation Rates From Simple 3-D Models of Mantle Convection. Geochem. Geophys. Geosystems 21. https://doi.org/10.1029/2019GC008809.
Lei, J., Zhao, D., 2007. Teleseismic evidence for a break-off subducting slab under Eastern Turkey. Earth Planet. Sci. Lett. 257, 14–28. https://doi.org/10.1016/j.epsl.2007.02.011.
Li, Z.H., Ribe, N.M., 2012. Dynamics of free subduction from 3-D boundary element modeling. J. Geophys. Res. Solid Earth 117, 1–18. https://doi.org/10.1029/2012JB009165.
Lim, J., Chang, S., Mai, P.M., Zahran, H., 2020. Asthenospheric flow of plume material beneath arabia inferred from s wave traveltime tomography. J. Geophys. Res. Solid Earth 125. https://doi.org/10.1029/2020jb019668.
Liu, M., Cui, X., Liu, F., 2004. Cenozoic rifting and volcanism in eastern China: a mantle dynamic link to the Indo-Asian collision? Tectonophysics 393, 29–42. https://doi.org/10.1016/j.tecto.2004.07.029.
Long, M.D., Silver, P.G., 2009. Shear wave splitting and mantle anisotropy: measurements, interpretations, and new directions. Surv. Geophys. 30, 407–461. https://doi.org/10.1007/s10712-009-9075-1.
Maggi, A., Priestley, K., 2005. Surface waveform tomography of the Turkish-Iranian plateau. Geophys. J. Int 160, 1068–1080. https://doi.org/10.1111/j.1365-246X.2005.02505.x.
Mahmoodabadi, M., Yaminifard, F., Tatar, M., Kaviani, A., 2020. Shear wave velocity structure of the upper-mantle beneath the northern Zagros collision zone revealed by nonlinear teleseismic tomography and Bayesian Monte-Carlo joint inversion of surface wave dispersion and teleseismic P-wave coda. Phys. Earth Planet. Inter. 300. https://doi.org/10.1016/j.pepi.2020.106444.
Mahmoodabadi, M., Yaminifard, F., Tatar, M., Kaviani, A., Motaghi, K., 2019. Upper-mantle velocity structure beneath the Zagros collision zone, Central Iran and Alborz from nonlinear teleseismic tomography. Geophys. J. Int 218, 414–428. https://doi.org/10.1093/gji/ggz160.
Mainprice, D., Barruol, G., Ismaïl, W.B., 2000. The seismic anisotropy of the Earth's mantle: from single crystal to polycrystal. American Geophysical Union,.
Manaman, N.S., Shomali, H., Koyi, H., 2011. New constraints on upper-mantle S-velocity structure and crustal thickness of the Iranian plateau using partitioned waveform inversion. Geophys. J. Int. 184, 247–267. https://doi.org/10.1111/j.1365-246X.2010.04822.x.
Mckenzie, D., 1972. Active Tectonics.
McKenzie, D., 1970. Plate Tectonics of the Mediterranean Region. Nature 226, 239–243.
McKenzie, D., 2010. The influence of dynamically supported topography on estimates of Te. Earth Planet. Sci. Lett. 295, 127–138. https://doi.org/10.1016/j.epsl.2010.03.033.
McKenzie, D., 2020. The structure of the lithosphere and upper mantle beneath the Eastern Mediterranean and Middle East. Mediterr. Geosci. Rev. 2, 311–326. https://doi.org/10.1007/s42990-020-00038-1.
McQuarrie, N., Van Hinsbergen, D.J.J., 2013. Retrodeforming the Arabia-Eurasia collision zone: Age of collision versus magnitude of continental subduction. Geology 41, 315–318. https://doi.org/10.1130/G33591.1.
Menant, A., Sternai, P., Jolivet, L., Guillou-Frottier, L., Gerya, T., 2016. 3D numerical modeling of mantle flow, crustal dynamics and magma genesis associated with slab roll-back and tearing: The eastern Mediterranean case. Earth Planet. Sci. Lett. 442, 93–107. https://doi.org/10.1016/j.epsl.2016.03.002.
Miller, M.S., Becker, T.W., 2012. Mantle flow deflected by interactions between subducted slabs and cratonic keels. Nat. Geosci. 5, 726–730. https://doi.org/10.1038/ngeo1553.
Mohammadi, E., Sodoudi, F., Kind, R., Rezapour, M., 2013. Presence of a layered lithosphere beneath the Zagros collision zone. Tectonophysics 608, 366–375. https://doi.org/10.1016/j.tecto.2013.09.017.
Mohammadi, N., Rahimi, H., Gholami, A., Pachhai, S., Aoudia, A., 2022. Shear-wave velocity structure of upper mantle along the Zagros collision zone. Tectonophysics 837. https://doi.org/10.1016/j.tecto.2022.229444.
Mohr, P., 1970. Afar triple junction and sea- floor spreading. J. Geophys Res 75, 7340–7352. https://doi.org/10.1029/jb075i035p07340.
Montelli, R., Nolet, G., Dahlen, F.A., Masters, G., 2006. A catalogue of deep mantle plumes: new results from finitefrequency tomography. Geochem. Geophys. Geosystems 7 (11). https://doi.org/10.1029/2006GC001248.
Montelli, R., Nolet, G., Dahlen, F.A., Masters, G., Engdahl, E.R., Hung, S.H., 2004. Finite-frequency tomography reveals a variety of plumes in the mantle. Science 303, 338–343. https://doi.org/10.1126/science.1092485.
Mortezanejad, G., Rahimi, H., Romanelli, F., Panza, G.F., 2019. Lateral variation of crust and upper mantle structures in NW Iran derived from surface wave analysis. J. Seismol 23, 77–108. https://doi.org/10.1007/s10950-018-9794-1.
Motaghi, K., Shabanian, E., Tatar, M., Cuffaro, M., Doglioni, C., 2017. The south Zagros suture zone in teleseismic images. Tectonophysics 694, 292–301. https://doi.org/10.1016/j.tecto.2016.11.012.
Moucha, R., Forte, A.M., 2011. Changes in African topography driven by mantle convection. Nat. Geosci. 4, 707–712. https://doi.org/10.1038/ngeo1235.
Mousavi, N., Fullea, J., 2020. 3-D thermochemical structure of lithospheric mantle beneath the Iranian plateau and surrounding areas from geophysical-petrological modelling. Geophys. J. Int. 222, 1295–1315. https://doi.org/10.1093/gji/ggaa262.
Mousavi, N., Fullea, J., Shafaii Moghadam, H., Griffin, W.L., 2023. Mantle compositional structure and dynamics of the Arabia-Eurasia collision zone: Insights from integrated thermochemical modelling. Gondwana Res 118, 37–57. https://doi.org/10.1016/j.gr.2023.02.011.
Mouthereau, F., 2011. Timing of uplift in the Zagros belt/Iranian plateau and accommodation of late Cenozoic Arabia-Eurasia convergence. Geol. Mag. 148, 726–738. https://doi.org/10.1017/S0016756811000306.
Movaghari, R., JavanDoloei, G., Yang, Y., Tatar, M., Sadidkhouy, A., 2021. Crustal radial anisotropy of the iran plateau inferred from ambient noise tomography. J. Geophys. Res. Solid Earth 126. https://doi.org/10.1029/2020JB020236.
Müller, R.D., Sdrolias, M., Gaina, C., Roest, W.R., 2008. Age, spreading rates, and spreading asymmetry of the world's ocean crust. Geochem. Geophys. Geosystems 9, 1–19. https://doi.org/10.1029/2007GC001743.
Nicolas, A., Christensen, N.I., 2011. Form. anisotropy Up. mantle peridotites: A Rev. 111–123. https://doi.org/10.1029/gd016p0111.
Nikogosian, I.K., Bracco Gartner, A.J.J., van Bergen, M.J., Mason, P.R.D., van Hinsbergen, D.J.J., 2018. Mantle sources of recent anatolian intraplate magmatism: a regional plume or local tectonic origin? Tectonics 37, 4535–4566. https://doi.org/10.1029/2018TC005219.
Omrani, J., Agard, P., Whitechurch, H., Benoit, M., Prouteau, G., Jolivet, L., 2008. Arc-magmatism and subduction history beneath the Zagros Mountains, Iran: a new report of adakites and geodynamic consequences. Lithos 106, 380–398. https://doi.org/10.1016/j.lithos.2008.09.008.
Pang, K.N., Chung, S.L., Zarrinkoub, M.H., Khatib, M.M., Mohammadi, S.S., Chiu, H.Y., Chu, C.H., Lee, H.Y., Lo, C.H., 2013. Eocene-oligocene post-collisional magmatism in the lut-sistan region, eastern iran: magma genesis and tectonic implications. Lithos 180–181, 234–251. https://doi.org/10.1016/j.lithos.2013.05.009.
Park, J., Levin, V., 2002. Seismic anisotropy: tracing plate dynamics in the mantle. Science 296.
Park, Y., Nyblade, A.A., Rodgers, A.J., 2007. Upper mantle structure beneath the Arabian Peninsula and northern Red Sea from teleseismic body wave tomography: Implications for the origin of Cenozoic uplift and volcanism in the Arabian Shield. https://doi.org/10.1029/2006GC001566.
Park, Y., Nyblade, A.A., Rodgers, A.J., Al-Amri, A., 2008. S wave velocity structure of the Arabian Shield upper mantle from Rayleigh wave tomography. Geochem. Geophys. Geosystems 9, 1–15. https://doi.org/10.1029/2007GC001895.
Paul, A., Karabulut, H., Mutlu, A.K., Salaün, G., 2014. A comprehensive and densely sampled map of shear-wave azimuthal anisotropy in the Aegean-Anatolia region. Earth Planet. Sci. Lett. 389, 14–22. https://doi.org/10.1016/j.epsl.2013.12.019.
Paul, A., Kaviani, A., Hatzfeld, D., Vergne, J., Mokhtari, M., 2006. Seismological evidence for crustal-scale thrusting in the Zagros mountain belt (Iran). Geophys. J. Int 166, 227–237. https://doi.org/10.1111/j.1365-246X.2006.02920.x.
Paul, A., Hatzfeld, D., Kaviani, A., Tatar, M., Péquegnat, C., 2010. Seismic imaging of the lithospheric structure of the Zagros mountain belt (Iran). Geol. Soc. Spec. Publ. 330, 5–18. https://doi.org/10.1144/SP330.2.
Piromallo, C., Morelli, A., 2003. *P* wave tomography of the mantle under the Alpine-Mediterranean area. J. Geophys. Res. Solid Earth 108, 1–23. https://doi.org/10.1029/2002JB001757.
Piromallo, C., Becker, T.W., Funiciello, F., Faccenna, C., 2006. Three-dimensional instantaneous mantle flow induced by subduction. Geophys. Res. Lett. 33, 5–8. https://doi.org/10.1029/2005GL025390.
Portner, D.E., Delph, J.R., Berk Biryol, C., Beck, S.L., Zandt, G., Özacar, A.A., Sandvol, E., Türkelli, N., 2018. Subduction termination through progressive slab deformation across Eastern Mediterranean subduction zones from updated P-wave tomography beneath Anatolia. Geosphere 14, 907–925. https://doi.org/10.1130/GES01617.1.
Priestley, K., McKenzie, D., Barron, J., Tatar, M., Debayle, E., 2012. The zagros core: deformation of the continental lithospheric mantle. Geochem. Geophys. Geosystems 13. https://doi.org/10.1029/2012GC004435.
Qaysi, S., Liu, K.H., Gao, S.S., 2018. A database of shear-wave splitting measurements for the Arabian plate. Seismol. Res. Lett. 89, 2294–2298. https://doi.org/10.1785/0220180144.
Rabayrol, F., Hart, C.J.R., Thorkelson, D.J., 2019. Temporal, spatial and geochemical evolution of late cenozoic post-subduction magmatism in central and eastern

Anatolia, Turkey. Lithos 336–337, 67–96. https://doi.org/10.1016/j.lithos.2019.03.022.
Rahimi, H., Hamzehloo, H., Vaccari, F., Panza, G.F., 2014. Shear-wave velocity tomography of the lithosphere–asthenosphere system beneath the Iranian plateau. Bull. Seismol. Soc. Am. 104, 2782–2798. https://doi.org/10.1785/0120130319.
Rahmani, M., Motaghi, K., Ghods, A., Sobouti, F., Talebian, M., Ai, Y., Chen, L., 2019. Deep velocity image of the north Zagros collision zone (Iran) from regional and teleseismic tomography. Geophys. J. Int 219, 1729–1740. https://doi.org/10.1093/gji/ggz393.
Reid, M.R., Delph, J.R., Cosca, M.A., Schleiffarth, W.K., Gençalioğlu Kuşcu, G., 2019. Melt equilibration depths as sensors of lithospheric thickness during Eurasia-Arabia collision and the uplift of the Anatolian Plateau. Geology 47, 943–947. https://doi.org/10.1130/G46420.1.
Reilinger, R.E., McClusky, S.C., Oral, M.B., King, R.W., Toksoz, M.N., Barka, A.A., Kinik, I., Lenk, O., Sanli, I., 1997. Global Positioning System measurements of present-day crustal movements in the Arabia-Africa-Eurasia plate collision zone. J. Geophys. Res. Solid Earth 102, 9983–9999. https://doi.org/10.1029/96jb03736.
Ribe, N.M., 1989. Seismic anisotropy and mantle flow. J. Geophys. Res. 94, 4213–4223. https://doi.org/10.1029/JB094iB04p04213.
Ricard, Y., Vigny, C., 1989. Mantle dynamics with induced plate tectonics. J. Geophys. Res. 94. https://doi.org/10.1029/jb094ib12p17543.
Ritsema, J., Van Heijst, H.J., Woodhouse, J.H., 1999. Complex shear wave velocity structure imaged beneath Africa and Iceland. Science 286, 1925–1931. https://doi.org/10.1126/science.286.5446.1925.
Ritsema, J., Deuss, A., Van Heijst, H.J., Woodhouse, J.H., 2011. S40RTS: A degree-40 shear-velocity model for the mantle from new Rayleigh wave dispersion, teleseismic traveltime and normal-mode splitting function measurements. Geophys. J. Int. 184, 1223–1236. https://doi.org/10.1111/j.1365-246X.2010.04884.x.
Robertson, A.H.F., 2000. Mesozoic-Tertiary tectonic-sedimentary evolution of a south Tethyan oceanic basin and its margins in southern Turkey.
Sadeghi-Bagherabadi, A., Margheriti, L., Aoudia, A., Sobouti, F., 2018. Seismic anisotropy and its geodynamic implications in Iran, the easternmost part of the tethyan belt. Tectonics 37, 4377–4395. https://doi.org/10.1029/2018TC005209.
Sadidkhouy, A., Javan-Doloei, G., Siahkoohi, H.R., 2008. Seismic anisotropy in the crust and upper mantle of the Central Alborz Region, Iran. Tectonophysics 456, 194–205. https://doi.org/10.1016/j.tecto.2008.05.001.
Salah, M.K., 2013. Seismic anisotropy structure beneath the southeastern Mediterranean from shear-wave splitting. Arab. J. Geosci. 6, 1717–1730. https://doi.org/10.1007/s12517-011-0480-7.
Salaün, G., Pedersen, H.A., Paul, A., Farra, V., Karabulut, H., Hatzfeld, D., Papazachos, C., Childs, D.M., Pequegnat, C., Afacan, T., Aktar, M., Bourova-Flin, E., Cambaz, D., Hatzidimitriou, P., Hubans, F., Kementzetzidou, D., Karagianni, E., Karagianni, I., Komec Mutlu, A., Dimitrova, L., Ozakin, Y., Roussel, S., Scordilis, M., Vamvakaris, D., 2012. High-resolution surface wave tomography beneath the Aegean-Anatolia region: Constraints on upper-mantle structure. Geophys. J. Int. 190, 406–420. https://doi.org/10.1111/j.1365-246X.2012.05483.x.
Sandvol, E., Turkelli, N., Barazangi, M., 2003. The Eastern Turkey seismic experiment: the study of a young continent-continent collision. Geophys. Res. Lett. 30, 1–2. https://doi.org/10.1029/2003GL018912.
Savage, M.S., 1999. Seismic anisotropy and mantle deformation: what have we learned from shear wave splitting. Rev. Geophys. 37, 65–106. https://doi.org/10.1029/98RG02075.
Sengör, A.M.C., Kidd, W.S.F., 1979. POST-COLLISIONAL TECTONICS OF THE TURKISH-IRANIAN PLATEAU AND A COMPARISON WITH TIBET.
Şengör, A.M.C., Özeren, S., Genç, T., Zor, E., 2003. East Anatolian High Plateau as a mantle-supported, north-south shortened domal structure. Geophys. Res. Lett. 30, 2–5. https://doi.org/10.1029/2003GL017858.
Şengör, A.M.C., Tüysüz, O., Imren, C., Sakinç, M., Eyidoğan, H., Görür, N., Le Pichon, X., Rangin, C., 2005. The north anatolian fault: a new look. Annu. Rev. Earth Planet. Sci. 33, 37–112. https://doi.org/10.1146/annurev.earth.32.101802.120415.
Şengör, C.A.M., Yilmaz, Y., 1981. TETHYAN EVOLUTION OF TURKEY: A PLATE TECTONIC APPROACH.
Şengül Uluocak, E., Oğuz, H., Pysklywec, G., Chen, B, R.N., 2021. Geodynamics of east anatolia-caucasus domain: inferences from 3d thermo-mechanical models, residual topography, and admittance function analyses. Tectonics 40. https://doi.org/10.1029/2021TC007031.
Serpelloni, E., Cavaliere, A., Martelli, L., Pintori, F., Anderlini, L., Borghi, A., Randazzo, D., Bruni, S., Devoti, R., Perfetti, P., Cacciaguerra, S., 2022. Surface velocities and strain-rates in the euro-mediterranean region from massive GPS data processing. Front. Earth Sci. 10. https://doi.org/10.3389/feart.2022.907897.
Shomali, Z.H., Keshvari, F., Hassanzadeh, J., Mirzaei, N., 2011. Lithospheric structure beneath the Zagros collision zone resolved by non-linear teleseismic tomography. Geophys. J. Int. 187, 394–406. https://doi.org/10.1111/j.1365-246X.2011.05150.x.
Silver, P.G., 1996. Seismic anisotropy beneath the continents: probing the depths of geology. Annu. Rev. Earth Planet. Sci. 24, 385–432. https://doi.org/10.1146/annurev.earth.24.1.385.
Silver, P.G., Chan, W.W., 1991. Shear wave splitting and subcontinental mantle deformation. J. Geophys. Res 96. https://doi.org/10.1029/91jb00899.
Silver, P.G., Holt, W.E., 2002. The mantle flow field beneath western North America. Science 295, 1054–1057.
Simmons, N.A., Myers, S.C., Johannesson, G., Matzel, E., 2012. LLNL-G3Dv3: Global P wave tomography model for improved regional and teleseismic travel time prediction. J. Geophys. Res. Solid Earth 117, B10302.
Skobeltsyn, G., Mellors, R., Gök, R., Türkelli, N., Yetirmishli, G., Sandvol, E., 2014. Upper mantle *S* wave velocity structure of the East Anatolian-Caucasus region: S wave structure of Anatolia-Caucasus. Tectonics 33, 207–221. https://doi.org/10.1002/2013TC003334.
Sleep, N.H., 1997. Lateral flow and ponding of starting plume material. J. Geophys. Res. Solid Earth 102, 10001–10012. https://doi.org/10.1029/97jb00551.
Smit, J., Brun, J.P., Cloetingh, S., Ben-Avraham, Z., 2010. The rift-like structure and asymmetry of the dead sea fault. Earth Planet. Sci. Lett. 290, 74–82. https://doi.org/10.1016/j.epsl.2009.11.060.
Stern, R.J., Johnson, P., 2010. Continental lithosphere of the Arabian Plate: a geologic, petrologic, and geophysical synthesis. Earth-Sci. Rev. 101, 29–67. https://doi.org/10.1016/j.earscirev.2010.01.002.
Sternai, P., Jolivet, L., Menant, A., Gerya, T., 2014. Driving the upper plate surface deformation by slab rollback and mantle flow. Earth Planet. Sci. Lett. 405, 110–118. https://doi.org/10.1016/j.epsl.2014.08.023.
Storchak, D.A., Di Giacomo, D., Bondár, I., Engdahl, E.R., Harris, J., Lee, W.H.K., Villaseñor, A., Bormann, P., 2013. Public release of the isc–gem global instrumental earthquake catalogue (1900–2009). Seismol. Res. Lett. 84, 810–815. https://doi.org/10.1785/0220130034.
Storchak, D.A., Di Giacomo, D., Engdahl, E.R., Harris, J., Bondár, I., Lee, W.H.K., Bormann, P., Villaseñor, A., 2015. The ISC-GEM Global Instrumental Earthquake Catalogue (1900-2009): Introduction. Phys. Earth Planet. Inter. 239, 48–63. https://doi.org/10.1016/j.pepi.2014.06.009.
Strak, V., Schellart, W.P., 2014. Evolution of 3-D subduction-induced mantle flow around lateral slab edges in analogue models of free subduction analysed by stereoscopic particle image velocimetry technique. Earth Planet. Sci. Lett. 403, 368–379. https://doi.org/10.1016/j.epsl.2014.07.007.
Styles, E., Goes, S., van Keken, P.E., Ritsema, J., Smith, H., 2011. Synthetic images of dynamically predicted plumes and comparison with a global tomographic model. Earth Planet. Sci. Lett. 311, 351–363. https://doi.org/10.1016/j.epsl.2011.09.012.
Styron, R., Pagani, M., 2020. The GEM global active faults database. Earthq. Spectra 36, 160–180. https://doi.org/10.1177/8755293020944182.
Talebian, M., Jackson, J., 2002. Offset on the main recent fault of nw iran and implications for the late cenozoic tectonics of the arabia-eurasia collision zone. Geophys. J. Int.
Tang, Z., Julià, J., Zahran, H., Mai, P.M., 2016. The lithospheric shear-wave velocity structure of Saudi Arabia: young volcanism in an old shield. Tectonophysics 680, 8–27. https://doi.org/10.1016/j.tecto.2016.05.004.
Tang, Z., Mai, P.M., Chang, S.J., Zahran, H., 2018. Evidence for crustal low shear-wave speed in western Saudi Arabia from multi-scale fundamental-mode Rayleigh-wave group-velocity tomography. Earth Planet. Sci. Lett. 495, 24–37. https://doi.org/10.1016/j.epsl.2018.05.011.
Tang, Z., Mai, P.M., Julià, J., Zahran, H., 2019. Shear velocity structure beneath Saudi Arabia from the joint inversion of P and S Wave receiver functions, and rayleigh wave group velocity dispersion. Data. J. Geophys. Res. Solid Earth 124, 4767–4787. https://doi.org/10.1029/2018JB017131.
Tsekhmistrenko, M., Sigloch, K., Hosseini, K., Barruol, G., 2021. A tree of Indo-African mantle plumes imaged by seismic tomography. Nat. Geosci. 14, 612–619. https://doi.org/10.1038/s41561-021-00762-9.
Tunini, L., Jiménez-Munt, I., Fernandez, M., Vergés, J., Bird, P., 2017. Neotectonic deformation in central eurasia: a geodynamic model approach. J. Geophys. Res. Solid Earth 122, 9461–9484. https://doi.org/10.1002/2017JB014487.
Turcotte, D.L., Oxburgh, E.R., 1972. MANTLE CONVECTION AND THE NEW GLOBAL TECTONICS.
Turcotte, D.L., Schubert, G., 2002. Geodynamics. Cambridge university press.
Van Benthem, S., Govers, R., 2010. The Caribbean plate: Pulled, pushed, or dragged? J. Geophys. Res. Solid Earth 115. https://doi.org/10.1029/2009JB006950.
van der Meer, D.G., van Hinsbergen, D.J.J., Spakman, W., 2018. Atlas of the underworld: Slab remnants in the mantle, their sinking history, and a new outlook on lower mantle viscosity. Tectonophysics 723, 309–448. https://doi.org/10.1016/j.tecto.2017.10.004.
Van Hinsbergen, D.J.J., Maffione, M., Plunder, A., Kaymakcit, N., Ganerød, M., Hendriks, B.W.H., Corfu, F., Gürer, D., De Gelder, G.I.N.O., Peters, K., McPhee, P.J., Brouwer, F.M., Advokaat, E.L., Vissers, R.L.M., 2016. Tectonic evolution and paleogeography of the Kbox drawings light down and leftrşehir Block and the Central Anatolian Ophiolites, Turkey. Tectonics 35, 983–1014. https://doi.org/10.1002/2015TC004018.
Veisi, M., Sobouti, F., Chevrot, S., Abbasi, M., Shabanian, E., 2021. Upper mantle structure under the Zagros collision zone; insights from 3D teleseismic P-wave tomography. Tectonophysics 819. https://doi.org/10.1016/j.tecto.2021.229106.
Vernant, P., Nilforoushan, F., Hatzfeld, D., Abbassi, M.R., Vigny, C., Masson, F., Nankali, H., Martinod, J., Ashtiani, A., Bayer, R., Tavakoli, F., Chéry, J., 2004. Present-day crustal deformation and plate kinematics in the Middle East constrained by GPS measurements in Iran and northern Oman. Geophys. J. Int 157, 381–398. https://doi.org/10.1111/j.1365-246X.2004.02222.x.
Wang, W., Becker, T.W., 2019. Upper mantle seismic anisotropy as a constraint for mantle flow and continental dynamics of the North American plate. Earth Planet. Sci. Lett. 514, 143–155. https://doi.org/10.1016/j.epsl.2019.03.019.
Wei, W., Zhao, D., Wei, F., Bai, X., Xu, J., 2019. Mantle Dynamics of the Eastern Mediterranean and Middle East: constraints from p-wave anisotropic tomography. Geochem. Geophys. Geosystems 20, 4505–4530. https://doi.org/10.1029/2019GC008512.
White, D.B., 1988. The planforms and onset of convection with a temperature-dependent viscosity (https://doi.org/DOI:). J. Fluid Mech. 191, 247–286. https://doi.org/10.1017/S0022112088001582.
Wolfe, C.J., Vernon, F.L., Al-Amri, A., 1999. Shear-wave splitting across western Saudi Arabia: the pattern of upper mantle anisotropy at a proterozoic shield. Geophys. Res. Lett. 26, 779–782. https://doi.org/10.1029/1999GL900056.

Wu, Z., Chen, L., Talebian, M., Wang, X., Jiang, M., Ai, Y., Lan, H., Gao, Y., Khatib, M.M., Hou, G., Chung, S.L., Liang, X., Zhao, L., Naimi-Ghassabian, N., Xiao, W., Zhu, R., 2021. Lateral structural variation of the lithosphere-asthenosphere system in the northeastern to eastern iranian plateau and its tectonic implications. J. Geophys. Res. Solid Earth 126. https://doi.org/10.1029/2020JB020256.

Wüstefeld, A., Bokelmann, G., Barruol, G., Montagner, J.P., 2009. Identifying global seismic anisotropy patterns by correlating shear-wave splitting and surface-wave data. Phys. Earth Planet. Inter. 176, 198–212. https://doi.org/10.1016/j.pepi.2009.05.006.

Yao, Z., Mooney, W.D., Zahran, H.M., Youssef, S.E.H., 2017. Upper mantle velocity structure beneath the Arabian shield from Rayleigh surface wave tomography and its implications. J. Geophys. Res. Solid Earth 122, 6552–6568. https://doi.org/10.1002/2016JB013805.

Yu, C., Chen, W., Van Der Hilst, R.D., 2016. Constraints on residual topography and crustal properties in the western United States from virtual deep seismic sounding. J. Geophys. Res. Solid Earth 121, 5917–5930. https://doi.org/10.1002/2016JB013046.

Zanchi, A., Zanchetta, S., Berra, F., Mattei, M., Garzanti, E., Molyneux, S., Nawab, A., Sabouri, J., 2009. The Eo-Cimmerian (Late? Triassic) orogeny in North Iran. Geol. Soc. Lond. Spec. Publ. 312, 31–55. https://doi.org/10.1144/SP312.3.

Zhang, Z., Karato, S., 1995. Lattice preferred orientation of olivine aggregates in simple shear". J. = Nat. Nat. 375, 774–777.

Zhong, S., Gurnis, M., 1995. Mantle convection with plates and mobile, faulted plate margins. N. Ser.

Zhu, R., Zhao, P., Zhao, L., 2022. Tectonic evolution and geodynamics of the Neo-Tethys Ocean. Sci. China Earth Sci. 65. https://doi.org/10.1007/s11430-021-9845-7.

Zor, E., 2008. Tomographic evidence of slab detachment beneath eastern Turkey and the caucasus. Geophys. J. Int 175, 1273–1282. https://doi.org/10.1111/j.1365-246X.2008.03946.x.

Zor, E., Sandvol, E., Gürbüz, C., Türkelli, N., Seber, D., Barazangi, M., 2003. The crustal structure of the east anatolian plateau (Turkey) from receiver functions: crustal structure from receiver functions. Geophys. Res. Lett. 30. https://doi.org/10.1029/2003GL018192.